

Ingvild Persson Moseby

# Experimental Studies of Flexible Propellers on a Marine Thruster

Master's thesis in Marine Technology  
Supervisor: Luca Savio  
June 2019



Ingvild Persson Moseby

# Experimental Studies of Flexible Propellers on a Marine Thruster

Master's thesis in Marine Technology  
Supervisor: Luca Savio  
June 2019

Norwegian University of Science and Technology  
Faculty of Engineering  
Department of Marine Technology

 **NTNU**  
Norwegian University of  
Science and Technology





---

**MASTER THESIS IN MARINE TECHNOLOGY**  
**SPRING 2019**  
**FOR**  
**Ingvild Persson Moseby**

Marine propellers made out of composite materials will be sufficiently flexible, making it possible to benefit from the mechanical properties to obtain a flexure that improves the propeller performance. Largest improvement is seen when the load increases, for example in an inhomogeneous wake field, the pitch is reduced.

The flexibility of the propellers will have to be taken into account when the performance is evaluated. When experimentally testing a model of this type of propeller, the modulus of elasticity must be smaller in model scale than the full scale structure.

It is produced three different resin casted propellers with different skew distribution used to test the performance of a flexible propeller. An open water test has been conducted on the propellers.

The core part the master thesis is to model test the flexible propellers on a thruster in the Towing Tank at SINTEF Ocean. The aims are to develop a plan, conduct the experiment and analyse the results of the model tests for three flexible propellers on different advance coefficients and azimuthing angles. A literature review will present the status of knowledge with respect to composite propellers. The candidate will design the thruster which shall be tested in a CAD program and decide the dimensions based on available knowledge.

Supervisor: Professor Luca Savio

Start: 15.01.2019

Deadline: 11.06.2019

---

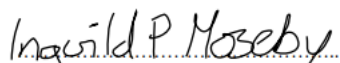
# Preface

This master thesis is written as a part of the degree Master in Science at the Norwegian University of Science and Technology and the Department of Marine Technology during the spring term in 2019. The thesis is performed as a part of the research project KPN FleksProp, which is a cooperation with NTNU, SINTEF Ocean and Kongsberg Maritime with financial support of the Norwegian Research Council.

The main part of the thesis is about model tests done in the towing tank at SINTEF Ocean with flexible propellers on a marine thruster. The resulting propeller performance and harmonics have been evaluated. A literature study and design of the open geometry thruster are also included in the scope of the thesis.

This thesis is a continuance of my project thesis which I wrote in the autumn term 2018. The scope has been altered, as it was decided that the model testing should be done with a marine thruster unit instead of tests in the cavitation tunnel. The subject was decided as a result of conversations with my supervisor and needs defined in the project scope of the research project FleksProp.

Special thanks is given to my supervisor Luca Savio for continuous guidance and support during the work, by sharing ideas and giving input on my work. I would like to thank Prof. Sverre Steen, who acted as the supervisor of my project thesis. I am grateful for the help from by SINTEF Ocean. Thanks to Nils Arne Snekvik for support with designing the thruster unit and Morten Korsvold for conducting the model tests. Finally, I would like to thank the members of the FleksProp research project who gave me guidance on application of composite material and input for further use of flexible propellers on marine thrusters.



Ingvild Persson Moseby  
Trondheim, 07.06.2019

---

# Summary

Marine propellers made of flexible materials have the possibility to enhance the performance by allowing the geometry to self-adapt to hydrodynamic load variations.

In cooperation with the research project FleksProp, model tests have been done for three propellers on a marine thruster at SINTEF Ocean in Trondheim. The propellers had a varying skew distribution and tests were done for both rigid and flexible propellers at three different azimuthing conditions. The changes in propeller performance and harmonic responses were evaluated.

The flexible propellers were made of isotropic resin. Bend-twist coupling occurred when the elastic axis of the propeller blade did not coincide with the center of pressure and changed the pitch angle.

A considerable change in performance was observed for the flexible propellers compared to the rigid propellers under various operation conditions. Similar differences between the rigid and flexible propellers were not observed for the harmonics.

The skew distribution had a significant influence on the hydroelastic behaviour which affected performance and harmonics of the propellers. The propeller without skew had twice as large relative difference between the rigid and flexible propeller thrust coefficients compared to the other propellers. For the harmonics, the propeller with balanced skew distribution had smaller changes in response for the increasing advance ratios compared to the other propellers.

The propeller performance and harmonics were altered in azimuthing conditions. The harmonic response increased at high advance ratios, and there was a greater spread between the response of the different propellers. The skew distribution influenced how the azimuthing angles affected the harmonic responses and propeller performance.

# Table of Contents

<b>Preface</b>	<b>ii</b>
<b>Summary</b>	<b>iii</b>
<b>Table of Contents</b>	<b>v</b>
<b>List of Tables</b>	<b>vi</b>
<b>List of Figures</b>	<b>viii</b>
<b>List of Abbreviations</b>	<b>ix</b>
<b>List of Symbols</b>	<b>x</b>
<b>1 Introduction</b>	<b>1</b>
1.1 Background . . . . .	1
1.2 Objective . . . . .	2
1.3 Structure of Thesis . . . . .	3
<b>2 Literature Review</b>	<b>4</b>
2.1 Bend-Twist Coupling of Composite Material . . . . .	4
2.2 Operational Characteristics . . . . .	6
2.2.1 Hydrodynamic Performance . . . . .	6
2.2.2 Cavitation . . . . .	7
2.3 Propellers Eigenfrequencies . . . . .	8
2.4 The Skew Angle's Influence on the Hydroelastic Behaviour . . . . .	9
2.5 Computational Research on Flexible Propellers . . . . .	10
2.6 Previous Experiments and Uncertainties . . . . .	10
2.6.1 Experiments Used for Validation Data . . . . .	11
2.6.2 Results from Experiments . . . . .	12
<b>3 Propeller Data</b>	<b>14</b>
3.1 Working Principle of Propellers . . . . .	14
3.2 Open Geometry Propellers . . . . .	16
3.2.1 Skew Distribution of the Propellers . . . . .	16

---

3.2.2	Manufacturing of the Propellers . . . . .	18
3.2.3	Viscoelastic Effects . . . . .	18
<b>4</b>	<b>Thruster Design</b>	<b>20</b>
4.1	Azimuth Propulsion . . . . .	20
4.1.1	Literature Review for Azimuth Propulsion Units . . . . .	21
4.2	Literature Regarding Thruster Design . . . . .	22
4.3	Design of Thruster . . . . .	24
4.3.1	FleksProp Open Geometry Thruster . . . . .	25
4.3.2	Comments Regarding Fleksprop Open Geometry Thruster . . . . .	26
<b>5</b>	<b>Propulsion Unit Open Water Test</b>	<b>27</b>
5.1	Open Water Test Procedure . . . . .	27
5.2	Experiment Set Up . . . . .	29
5.2.1	Measurements . . . . .	33
5.2.2	Experiment Procedure . . . . .	34
5.2.3	Data Acquisition . . . . .	35
5.2.4	Processing of the Results . . . . .	36
<b>6</b>	<b>Results</b>	<b>39</b>
6.1	Evaluation of Possible Viscoelastic Effects . . . . .	39
6.2	Propeller Performance . . . . .	40
6.2.1	Repeatability of the Propeller Performance . . . . .	41
6.2.2	Open Water Curves . . . . .	42
6.2.3	Relative Difference Between Rigid and Flexible Propeller . . . . .	44
6.2.4	Relative Difference For Varying Heading Angles . . . . .	47
6.2.5	The Thruster Units Influence on the Performance . . . . .	51
6.3	Propeller Harmonics . . . . .	52
6.3.1	Harmonic Response and Corresponding Spectrum . . . . .	53
6.3.2	The Advance Ratios Influence on the Harmonics . . . . .	55
6.3.3	The Harmonics of the Repeating Runs . . . . .	57
6.3.4	Harmonics for Both Propeller Rotational Speeds . . . . .	58
6.3.5	Influence of Skew Angle on Harmonics . . . . .	59
6.3.6	Harmonics for Rigid Propellers Compared to Flexible Propellers . . . . .	61
6.3.7	Harmonics at Azimuthing Headings . . . . .	63
6.3.8	General Comments Regarding Larger Values in Response . . . . .	65
<b>7</b>	<b>Conclusion</b>	<b>67</b>
7.1	Further Work . . . . .	68
	<b>Bibliography</b>	<b>69</b>
	<b>Appendix</b>	<b>75</b>
7.2	Propeller Geometry . . . . .	75
7.2.1	P1374 . . . . .	75
7.2.2	P1565 . . . . .	76
7.2.3	P1566 . . . . .	77
7.2.4	Blade Section Profiles for P1374, P1565, P1566 . . . . .	78
7.3	Channel List . . . . .	79
7.4	Run Matrix . . . . .	80
7.5	Symbols used for the Results . . . . .	81

---

# List of Tables

3.1	Propeller Geometry . . . . .	16
4.1	Dimensions Limitations . . . . .	24
4.2	Dimensions Thruster . . . . .	25
5.1	Dimensions Towing Tank . . . . .	30
5.2	Operational Conditions . . . . .	35
6.1	Changes in Bollard Condition for P1566 . . . . .	40
6.2	Occurrences of Peaks in Spectra . . . . .	55
7.1	Main Geometrical Parameter of Propeller P1374 . . . . .	75
7.2	Main Geometrical Parameter of Propeller P1565 . . . . .	76
7.3	Main Geometrical Parameter of Propeller P1566 . . . . .	77

# List of Figures

3.1	Propeller Dimensions, figure taken from Steen (2014a) . . . . .	14
3.2	Hydrodynamic Loading of a Propeller, picture taken from Steen (2014a) . . . . .	15
3.3	Skew Distribution . . . . .	17
3.4	Outline of the Propeller Blades . . . . .	17
3.5	Viscoelastic Deformation . . . . .	19
4.1	Pushing and Pulling Configuration-Picture taken from Steen (2014a)	21
4.2	Thruster Dimensions, figure is modified from Molloy et al. (2006)	23
4.3	Thruster Unit Model Design in Rhinoceros . . . . .	26
4.4	3D Printed Version of the Thruster Unit . . . . .	26
5.1	Carriage with the Propulsion Unit in the Towing tank . . . . .	29
5.2	Set up of Propulsion Unit . . . . .	30
5.3	Thruster Unit with Propeller P1374AA . . . . .	31
5.4	Digital Set up of Propulsion Unit . . . . .	32
5.5	Set Up Seen from Above . . . . .	34
5.6	Stable Regions of the Speed for P1374AR . . . . .	37
5.7	RAOs for P1374AA and P1374AR . . . . .	37
6.1	Open Water Diagram for Three Successive Runs for P1374AR . .	41
6.2	Open Water Diagrams for P1374 . . . . .	42
6.3	Open Water Diagrams for P1565 . . . . .	43
6.4	Open Water Diagrams for P1566 . . . . .	43
6.5	Relative Difference of Thruster Unit Thrust Coefficient in Straight Ahead Condition . . . . .	45
6.6	Relative Difference of Torque Coefficient in Straight Ahead Condition . . . . .	45
6.7	Relative Difference in Propeller Thrust Coefficient in Straight Ahead Condition . . . . .	46

---

6.8	Force Directions . . . . .	48
6.9	Comparison of Propeller Thrust Coefficient for Varying Heading Angles . . . . .	49
6.10	Relative Difference of Unit Thrust Coefficients for Azimuth Angles	50
6.11	Difference in Performance for Propeller and Thruster Unit Open Water Tests . . . . .	52
6.12	Harmonic Response and Corresponding Spectrum for P1374AR .	54
6.13	Harmonic Response of the Different Advance Ratios for P1566AR	56
6.14	Harmonic Response for P1374AR with Changing Advance Ratios	56
6.15	Harmonics for P1374AR for Repeating Runs . . . . .	57
6.16	Harmonic Response for P1565AR at Speed 7 and 12 rps . . . . .	58
6.17	Harmonic Response for P1374AR at Speed 7 and 12 rps with Ad- vance Ratios . . . . .	59
6.18	First Harmonic for all Propellers at Zero Heading . . . . .	60
6.19	Harmonic Response for all Propellers at Zero Heading . . . . .	60
6.20	Harmonic Response for all Rigid Propellers . . . . .	61
6.21	Harmonic Response for Rigid and Flexible Propellers . . . . .	62
6.22	Deviation between Rigid and Flexible Propellers Harmonics at Zero Heading Angle . . . . .	62
6.23	Harmonic Response for P1566AR at all Azimuth Headings . . . . .	63
6.24	Harmonic Response based on Propeller Thrust for all Propellers .	64
6.25	Deviation Between Rigid and Flexible Harmonic Response in Az- imuth Conditions . . . . .	64
6.26	RAOs in FX for propeller P1565AR and P1566AR . . . . .	66
6.27	Three Repetitions for P1374AR . . . . .	66



---

# List of Abbreviations

FSI	Fluid Structure Interaction
ITTC	International Towing Tank Conference
MAB	Manganese-Aluminium Bronze
NAB	Nickel-Aluminium Bronze
FPP	Fixed Pitch Propeller
RANS	Reynolds Averaged Navier Stokes
BEM	Boundary Element Method
CFD	Computational Fluid Dynamics
RAO	Response Amplitude Operator

---

# List of Symbols

$J_A$	Advance coefficient
Rn	Reynolds number
Fn	Froude number
V	Velocity
n	Rotational speed
D	Propeller diameter
R	Propeller radius
P/D	Pitch to diameter ratio
$\phi$	Geometric pitch angle
$\beta_i$	Hydrodynamic pitch angle
$\rho$	Density of water
$\nu$	Kinematic viscosity
T	Thrust
$K_T$	Thrust coefficient
Q	Torque
$K_Q$	Torque coefficient
$\eta$	Efficiency
$\sigma$	Cavitation number
L	Characteristics length
g	Gravity coefficient
dL	Section lift force
dD	Section drag force
G	Shear modulus
E	Young modulus
$\nu$	Poisson ratio

# Introduction

Interest in use of composite material for marine propellers has increased in the last decade. These propellers utilize the material properties to benefit from hydroelasticity and are classified to be flexible. The flexibility alters the performance of the propeller.

## 1.1 Background

Traditionally, marine propellers are made of manganese-aluminum bronze, MAB, or nickel-aluminium bronze, NAB, and are considered to be rigid. These propellers have an excellent corrosion resistance, high yield strength, reliability and affordability, but, mentioned by Young (2008), struggle with corrosion fatigue, poor acoustic damping and cavitation damage. For fixed pitch propellers, FPP, commonly used for marine vessels, the propeller performance is optimized for one design condition. In off-design condition, as during acceleration, maneuvering and shallow water operation, the performance is reduced.

Flexible propellers made of composite materials have, according to Maljaars & Kaminski (2015), a reduced corrosion risk, weight and vibration due to more acoustic damping compared to MAB or NAB propellers. For these propellers, the deformation due to the bend-twist coupling can not be ignored, which can offer additional benefits to the performance. The fibers of the material can be tailored such that the propeller pitch passively adapts to the hydrodynamic load variations. Motley et al. (2009) explained that this self adapting pitch can improve the ef-

iciency, increase the cavitation inception speed and reduce noise and vibration. This is particular beneficial for operation in a spatial varying wake, which occurs behind a ship hull. In a spatial varying wake, the flow condition changes during a propeller revolution. The flexible propeller can instantaneously benefit from the bend-twist coupling, and the load variations can be reduced.

Azimuth propulsion units provide both propulsion and steering functions. According to Carlton (1994), it is becoming more common to use thrusters as the main propulsion for ships due to their dynamic positioning and manoeuvring capabilities. An azimuth propulsion unit can operate with an angle relative to the ship velocity. Amini et al. (2010) reported that thruster units have a different mechanical response than conventional propellers due to their short and vertical shaft. The complexity of the propeller, strut and pod interactions increase in azimuthing conditions.

## 1.2 Objective

This thesis describes model tests done with different flexible propellers on a marine thruster unit at SINTEF Ocean during the spring of 2019. The thruster body was tested with three different propellers for which the skew distribution changed. A rigid variants made of aluminium and a flexible variants made of resin were tested. The flexible propellers were made of an isotropic material. Different skew distributions were used as it should have a distinct influence on the bend-twist coupling for flexible propellers and thus the performance. The propellers have not been optimized to improve the propeller performance.

This thesis aims to evaluate the performance and harmonic response of the propulsion unit with the different flexible propellers. The performance changed between the flexible and rigid propellers, and in different azimuthing conditions. The results of this model test can be used as validation data for numerical research.

These objectives were decided as a limited number of validation data are available. Several publications have focused on flexible propellers, but the sensitivity of the propeller geometry on the hydroelastic behaviour has scarcely been evaluated. Few studies have been done for flexible propeller on thrusters. Thruster propulsion units have different mechanical responses compared to conventional propellers, which can affect the response of flexible propellers.

The tests were performed as a part of the research project FlexProp. It is a cooperation between SINTEF Ocean, Kongsberg Maritime and NTNU with financial support of the Norwegian Research Council. The goal of FlexProp is to build knowledge on how marine propulsors can be designed to utilize the elasticity to improve their reliability and possibly improve their performance.

### **1.3 Structure of Thesis**

The thesis consists of a literature review, design of an open geometry thruster, a model test in the towing tank and post processing of the results.

The literature review in chapter 2 presents the current state of knowledge on flexible marine propellers. The three propellers used for the model test are presented in detail in chapter 3. An open geometry thruster was designed as a part of the thesis, and the thruster geometry and the approach of the design are explained in chapter 4. Chapter 5 describes the procedure of the model test and the set up of propulsion unit and measurement equipments. The open water characteristics and harmonic responses of the propellers are shown in chapter 6, which post-process the results. Due to the amount of results, discussion and comments of the results follow the subsection which presents them.

# Literature Review

This section presents the research on propellers made of flexible material. The focus is on literature which is of relevance for model testing on flexible propellers and their operation.

## **2.1 Bend-Twist Coupling of Composite Material**

Hydroelasticity is interactions between a structure and a fluid medium which causes deformations of the structure. Abramson (1967) defined it more precisely as the phenomena involving mutual interactions between inertial, hydrodynamic and elastic forces acting on submerged or partially submerged elastic structural components. For ordinary fluid dynamic problems, the forces from to the fluid medium are too small to impact the rigid body. For elastic structures, as propellers made of composite materials, the forces are not negligible and the deformation must be taken into account.

For flexible propellers, the hydroelastic effect occurs through a bend-twist coupling. The bend-twist coupling means that the structure twists when it bends. For marine propellers, Lin et al. (2009) explained that this coupling would alter the pitch angle for the varying pressure distribution, thus changing the thrust, torque and efficiency. By tailoring the fiber of the composite material, the propeller pitch can passively self adapt to the hydrodynamic load variations. Compared to conventional marine propellers, flexible propellers therefore have the additional benefit to control the blade deformation to improve the propeller performance.

Isotropic materials are materials for which the properties at any point are the same in all direction. Bend-twist coupling occurs for propellers made of isotropic materials when the center of pressure is away from the elastic axis, or shear center, of the lifting body. Savio & Koushan (2019) stated that it is in theory possible to control the bend twist coupling of an isotropic blade by changing the relative location of the blade elastic axis and the center of pressure. This could be done by altering on the skew distribution, but this would significantly affect the cavitation behaviour of the propeller. Due to the dependency of the flow condition and load distribution, Young et al. (2018) stated that it is difficult to control the center of pressure and to vary the elastic axis. Consequently, tailoring the bend-twist coupling and enhancing the performance are challenging, if not impossible, when the propellers are produced with isotropic material.

For anisotropic materials, the material properties change with the directions. Bend-twist coupling occurs when the lamination scheme is unbalanced, meaning an unequal number of plies in the different directions. The unbalanced ply distribution decomposes the applied pressure in different directions causing the bend-twist coupling. Khan et al. (2000) showed how the bend-twist coupling of anisotropic material and corresponding propeller characteristics were significantly influenced by the stacking sequence and the ply orientation. Liu & Young (2007) evaluated the effect on the bend-twist coupling of increased number of layering, which was observed to decrease the degree of anisotropy, leading to less deformation.

Lin et al. (2009) evaluated propellers with quasi-isotropic and anisotropic stacking sequence. The deflection and the performance enhancement were greater for the anisotropic blade. The deflection of the blade was dependent on the rotational speed and was greater for an increased speed. The greatest deflection occurred at the blade tip.

Young et al. (2018) examined the flow induced twist for different loading and stacking sequence of the material. The flow induced twist increased for higher loading, and the performance was dependent on the direction of twist. Nose up twist increased the load and accelerated stall, flow separation and static divergence of the flow, whereas opposite occurred for nose-down twist. For isotropic materials, nose up twist occurred when the center of pressure was upstream the elastic axis. Material failure and flow-induced vibrations may occur before stall, which would change the performance. Das & Kapuria (2016) mentioned the importance

of considering material failure when evaluating the bend-twist coupling performance.

Several papers have evaluated the bend-twist coupling and tailoring methods to enhance the performance. There is a lack of papers evaluating possible failures of material and flow-induced vibrations which would considerably alter the performance.

## **2.2 Operational Characteristics**

The main objective for use of flexible propeller is the possibility to improve the operational characteristics by enhancing the hydrodynamic performance, delaying the cavitation inception and reducing the impact of the propeller on the surroundings.

### **2.2.1 Hydrodynamic Performance**

Publications agree that flexible propellers could lead to an efficiency enhancement compared to rigid propeller. However, there is a scatter in the proclaimed efficiency enhancement. Maljaars & Kaminski (2015) stated that the highest efficiency improvement declared in publications is up to 5% and the lowest is less than 1%.

The bend-twist coupling effects and the load-dependent self-adaption behaviour of the propeller blades are the primary sources for the efficiency enhancement. The propeller blades adjust the pitch with the hydrodynamic loads, making the propeller able to operate close to its optimal configuration for a larger range of operation conditions. Young (2008) postulated that the deformed propeller should match the optimal rigid propeller at the design condition. For lower advance ratios, thus higher hydrodynamic loading, the composites should allow the pitch near the blade tip to be lower than its rigid counterpart. For increased advance ratios, the pitch should self adjust to be higher than its rigid counterpart. Motley et al. (2009) evaluated the performance of a flexible propeller compared to a rigid propeller and observed that this self adjustment made the flexible propeller perform as the rigid propeller in design condition and better in off-design condition. Typical off-design condition are operation in shallow water, dynamic positioning, manoeuvring, turning and acceleration. This publication also evaluated the propeller in unsteady flow



operation and observed that for the self-twisting propellers, the time-averaged hydrodynamic forces were close to the operation in steady inflow. Also in unsteady flow did the flexible propeller perform as its rigid counterpart at design condition and had a performance enhancement in off-design condition.

A similar conclusion was drawn in other publications, as Young (2008) and Lee et al. (2015).

### 2.2.2 Cavitation

There is limited knowledge about the cavitation behaviour of flexible propellers and more research is necessary. Research done for cavitation behaviour of flexible propellers have mainly been done numerical. Maljaars & Kaminski (2015) stated that there are difficulties with implementation of cavitation in the fluid structure interaction, FSI, solver. There are uncertainties if the cavities will remain stable for transient blade vibration which can occur in spatial varying wakes. Even though the knowledge about cavitation behaviour for flexible propellers is limited, the number of independent publications with similar conclusion confirm a possible cavitation reduction.

Taketani et al. (2013) found by numerical and experimental approach that the elastic deformation of the material unloaded the propeller blade tip which reduced the cavitation volume on the blade. Maljaars & Kaminski (2015) used the de-pitching behaviour to observe that the cavitation inception speed increased for a flexible propeller. By decreasing the tunnel pressure in cavitation tunnel experiments, Huang et al. (2016) had a similar conclusion, the cavitation inception pressure decreased for a composite propeller. Hong et al. (2017) concluded alike when the cavitation number at maximum efficiency was evaluated. The cavitation number,  $\sigma$ , was observed to be significantly higher for composite propellers. Young (2008) stated that due to unstable cavities at the inception point, cavitation inception may not occur at the same speed for all propeller blades.

Huang et al. (2016) analyzed the cavitation performance of a composite propeller in a non-uniform flow. The cavitation bucket was wider for the composite propeller than for the metal propeller. This means that the range of cavitation-free operation was greater. Due to the deformation of the propeller blade, the pressure distribution was more uniform for the composite propeller. This caused the

tip vortex cavitation to occur before suction side sheet cavitation. This is the opposite of what occurred for the metal propeller, and the author stated it showed a performance improvement.

Motley et al. (2009) analyzed the thrust and efficiency breakdown due to sheet cavitation, and it was seen that at the same cavitation number, a higher breakdown occurred for the rigid propeller. The cavitation patterns for the propellers were similar, but the flexible propeller had a later cavitation inception with a reduced extent of face side sheet cavitation. This was proposed as an explanation for the difference in behaviour.

Maljaars & Dekker (2015) stated that it is possible to benefit from the low material density of composites to have thicker propeller blades and therefore increasing the cavitation inception speed. Due to the low weight of the material, no significant negative effects should occur. No research is mentioned which verifies this statement.

More research and observations of the cavitation behaviour for a flexible propeller are necessary. There is a need for more experimental approach to verify the implementation in the numerical solver.

## **2.3 Propellers Eigenfrequencies**

The propeller eigenfrequencies are reduced for composite propeller compared to rigid propellers, which increases the risk for resonance and load amplification. The range of excitation frequencies must be examined so the propeller is not susceptible for near-resonant blade vibration during operation. The encounter frequencies are easily obtained in a homogeneous wake field, but in a spatial varying or cavitating wake field, a Fourier transformation is necessary .

Lin & Tsai (2008) studied the free vibrations characteristics of composite propellers, and the degree of anisotropy was seen to affect the mode shapes. They proposed that a higher degree of anisotropy could alter the eigenfrequencies. The mode shapes were similar in air and in water. However, water immersion affected the natural frequency due to the added mass effects. The added mass effects were almost equal for the composite propeller as for the rigid propeller. The mode shapes and the added mass effects on the eigenfrequencies of composite propellers were also examined by Young (2008).

Motley et al. (2009) stated that a dynamic analysis should be used to design the composite propeller. The excitation frequencies could be altered to be much lower than the eigenfrequencies in water while also maintaining stability for a range of hydrodynamic conditions.

The eigenfrequencies impact on the performance and reliability of the composite propellers are of great importance. Their influence is difficult to take into account, especially for encounter frequencies in the range of the eigenfrequencies. The limited research of the effect on the propeller performance demonstrates the need for more knowledge of the dynamic characteristics of composite propellers in order to avoid resonant blade vibration or fatigue problems. This thesis starts to shed some light on the influence of eigenfrequencies by acquiring background information on the magnitude of excitation.

## **2.4 The Skew Angle's Influence on the Hydroelastic Behaviour**

The skew angle has a pronounced effect on the performance of the propeller.

Research done on rigid propellers by Ghassemi (2009) showed that a highly skewed propeller had lower thrust and torque fluctuations. Propeller skew could be used to reduce propeller-excited vibrations.

Ghassemi et al. (2012) examined the effect of the skew angle for composite propellers with anisotropic stacking. It was observed that it affected the deflection, stress field and propeller performance. The maximum deflection increased for larger skew angles. For all skew angles, deflection decreased for increased advance ratios. The deformation increased towards the blade tip due to the increased centrifugal force and hydrodynamic pressure. A larger skew angle led to lower thrust and torque performance for all values of the advance ratio. The efficiency of the deformed propeller blade was seen to be highest for zero skew angle. The difference in performance between flexible and rigid propellers was greater for large skew angles at high advance coefficients. The variations in propeller characteristics differed significantly for the different propellers.

Maljaars & Dekker (2015) evaluated isotropic propellers and stated that they found similar results as Ghassemi et al. (2012). They explained the behaviour

by a movement of the point of application of the net hydrodynamic force over the propeller blade due to changing advance ratios. For low advance ratios, the thrust is generated close to the leading edge, and it moves towards the trailing edge for increasing advance coefficients. This movement, especially for highly skew propellers, causes a de-pitching moment.

These publications suggest a high dependency on the propeller geometry on its flexibility. There are a scarce number of publications concerning this topic, suggesting a need for more research.

## **2.5 Computational Research on Flexible Propellers**

Most research done for flexible propellers have been done numerically. Due to the material properties of the composite material, computational research on these propellers requires that the fluid structure interaction, FSI, is correctly implemented.

FSI is interactions between a deformable or movable structure and an internal or surrounding flow. The fluid flow field will deform the physical structure, which in turn will change the flow field. An iteration loop for each time step is necessary until the deformation has converged. FSI can be implemented by strong or weak coupling and Zhang & Hisada (2004) examined the use of these different methods. For the strong coupling method, the variables are solved and corrected simultaneously. For the weak coupling method, the fluid and structural parts are solved sequentially and some variables are exchanged between the solvers, satisfying the interface conditions in an iterative manner. The weak coupling has the benefit of using existing solvers, and Maljaars & Kaminski (2015) mentioned that the large majority of publications have used this FSI implementation method.

## **2.6 Previous Experiments and Uncertainties**

Few experiments have been done for flexible propellers, and publications have mainly focused on numerical efforts. It is therefore a need for more experimentally based evidence for the improved properties of composite propellers presented in literature. The scarce number of model tests also suggest a lack of validation data for numerical efforts on flexible propeller. Maljaars & Kaminski (2015) mentioned that a majority of the hydroelastic couplings for propeller analysis are not

validated, and the lion's share of the validation data are for uniform wakes.

Savio & Koushan (2019) pointed at the scaling laws and difficulties to control the mechanical properties in production as the limitations for an experimental approach for flexible propellers. Experiments have been done in both towing tanks and cavitation tunnels. The most common objectives are validating the numerical analysis, as done by Lin et al. (2009), evaluate the performance characteristics, as by Paik et al. (2013), and verifying the measurement techniques, as Savio (2015).

### 2.6.1 Experiments Used for Validation Data

For several of the validation studies on FSI coupling with model tests, there is a deviation between the measurements and numerical results.

Nieminen (2017) and Young (2008) both explained misdoings in the propeller manufacturing as a possible reason for the deviation. Savio (2015) tested a 3D printed flexible propeller, and Nieminen (2017) stated that this approach could have produced material defects impacting the homogeneity, non-linearity and anisotropy. The propellers used for the experiment by Young (2008) had a different flexibility than determined in the design criterion, which was due to difficulties in the design and manufacturing process. It is difficult to verify the material properties after the manufacturing of the propeller, and as the results are sensitive to these properties, there are high requirements to the manufacturing process. In general, Maljaars et al. (2018) described that the composite material is difficult to implement numerical and therefore recommend to begin validating the FSI analysis with isotropic materials. Lin et al. (2009) proposed that the deviations for the results occurred from other factors, as the fluid flow and blade and shaft vibration on the measurements. Taketani et al. (2013) concluded from their comparison that the FSI analysis could estimate rather precise results for small propeller blade deformations, but proved relatively inaccurate for larger deformations.

Challenges also arose for the numerical approaches. Maljaars et al. (2018) mentioned that the uncertainties in the numerical codes could be a possible reason for the deviation. It can be difficult for fluid solvers to implement the flow separation which can occur at low advance ratios and viscous forces which can be dominating at higher advance ratios.

The majority of the publications concluded that the numerical results were val-

idated based on the experiments. The propeller performance was usually used as the validation parameter, but Maljaars & Kaminski (2015) suggested that propeller deflection is a better parameter. The propeller torque and thrust are easily influenced by other parameters, and their accuracy is in the same magnitude as the measurement accuracy. However, it is complicated to measure the deformations of a rotating propeller shown by the number of research which did not manage to have correct measurements. Young (2008) used laser tracking technique, which was later stated by Maljaars & Kaminski (2015) to have too low accuracy to predict the changes in the pitch deformation. Taketani et al. (2013) found it problematic to accurately estimate the deflection for small material deformation.

Measurements of the deflection is not necessarily included in the scope of the research and is therefore not possible to use as a validation parameter for all experiments. Having accurate validation parameters is a complicated task and can not be generalized to be valid for all studies. Validation studies should examine the accuracy of their parameters before concluding and presenting their results.

### **2.6.2 Results from Experiments**

The experiments done for flexible propellers have a wide range of objectives, and the findings are therefore varied.

Taketani et al. (2013) concluded from the experiment that the deformation increased for elastic material. In general, this reduced the propeller thrust and torque and the degree of deformation determined its effect on the propeller efficiency. It was indicated that there is an optimal level of deformation. At a certain point, the propeller efficiency began to decline with greater deformation. Pressure sensors were located above the propeller, and the fluctuating pressure were measured and seen to reduce for a flexible propeller.

Paik et al. (2013) measured the sound pressure level from the propeller, and the acoustic properties was observed to be dependent on the tailoring method. It increased for higher thrust and torque or occurrence of tip vortex cavitation. Young (2008) examined the strength of the tip vortex, which was seen to decrease for flexible propellers.

Savio (2015) stated that the most notable effect for the experiment was a backwards bending of the blade tip when the load was close to zero. The blade tip was

seen to have an increasing deflection for higher load, and the deflection was larger at the leading edge.

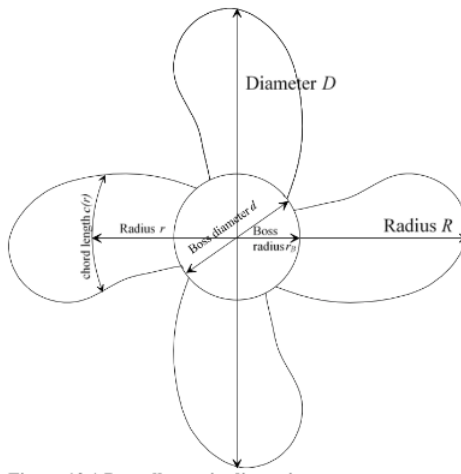
Young (2008) evaluated the stress distribution on the propeller blades for different tailoring methods. The stress distribution was seen to have a dependency on the material composition and layering sequence. This is important to consider when determining the operation range of the propellers to avoid material failure.

# Propeller Data

## 3.1 Working Principle of Propellers

This section is based on literature from Carlton (1994) and Harvald (1983).

The main dimensions of a propeller are seen in figure 3.1. A propeller is in addition described by its thickness, skew, rake and pitch distribution.



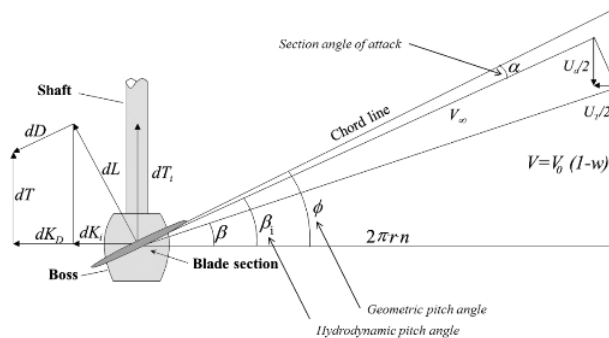
**Figure 3.1:** Propeller Dimensions, figure taken from Steen (2014a)

Figure 3.2 shows the working principle of a propeller. This approach is a simplified approach. In reality, the propeller performance is dependent on several parameters, as viscous effects, cavitation, number of blades, thickness and cham-



ber distribution. This section shows how the propeller performance is dependent on the angle of attack,  $\alpha_i$ , of each propeller blade section. This parameter will be affected when operating with flexible propeller blades.

The angle of attack is the difference between the geometrical pitch angle  $\phi$ , which is dependent on the propeller geometry, and the hydrodynamic pitch angle  $\beta_i$ , which is dependent on the incident flow. The resulting velocity,  $V_\infty$ , induces a lift force,  $dL$ , and a drag force,  $dD$  on each blade section. The section thrust,  $dT$ , is found by the contributions of lift and drag forces in axial direction. The section torque,  $dQ$ , is derived from the force contributions in tangential direction,  $dK$ , multiplied with the sectional radius  $r$ . The overall thrust and torque are determined by integrating each sections contribution.



**Figure 3.2:** Hydrodynamic Loading of a Propeller, picture taken from Steen (2014a)

As shown, the hydrodynamic performance is dependent on the pitch angle  $\phi$ . For the rigid propeller, the propeller pitch is designed such that optimal propeller performance occurs at the design flow condition. For the flexible propeller, the geometrical pitch angle is dependent on the inflow condition. It can vary radially to keep the angle of attack,  $\alpha$ , close to optimal position for all radial positions also in off-design conditions. The hydrodynamic performance of the propeller can thus be improved.

A body in a fluid field, as a vessel, causes a wake field with an uneven flow velocity distribution. The inflow wake field of the propeller is asymmetric due to hull-propeller interactions. As the angle of attack is changed with the variations of the inflow conditions, the hydrodynamic loading of the propeller has large fluctuations during one revolution. If the flexible propeller blade can change its pitch

distribution during each revolution in uneven wake fields, it would improve the performance.

## 3.2 Open Geometry Propellers

The open geometry propellers P1374, P1565 and P1566 were tested. The propellers are designed by SINTEF Ocean. Propeller P1374 is the parent geometry from which the other propellers have been derived. A large amount of numerical and experimental research have been done for this propeller and are available to the public.

The propellers have identical geometry, except for the skew distribution. The geometry can be seen in table 3.1. P1374 has a balanced skew of 23 degrees, P1565 has no skew and P1566 has an unbalanced skew of 23 degrees. The propellers are right handed. The skew distribution is shown in figure 3.3.

**Table 3.1:** Propeller Geometry

<b>Propeller Diameter</b>	250.00 [mm]
<b>Hub Diameter</b>	60.00 [mm]
<b>Number of Blades</b>	4
<b>Expanded Area Ratio</b>	0.602
<b>Design P/D</b>	1.1

The outline of the different propeller blades are seen in figure 3.4.

More details of the propeller geometry are shown in appendix 7.2.

### 3.2.1 Skew Distribution of the Propellers

Propeller skew is when the fixed line drawn through the shaft centre line does not coincide with the line going through the mid-chord point of the blade sections.

Section 2.4 presented the scarce research done on the skew distributions influence of the hydroelastic behaviour. It was shown that the pressure center on the propeller blade and elastic axis of the propeller blade were dependent on the skew distribution. The propellers used for these model tests are made with an isotropic material. Bend-twist coupling for isotropic material is discussed in section 2.1. It

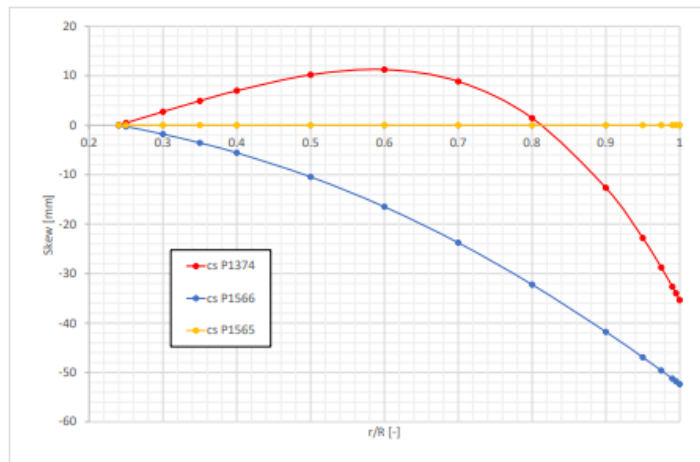


**Figure 3.3:** Skew Distribution

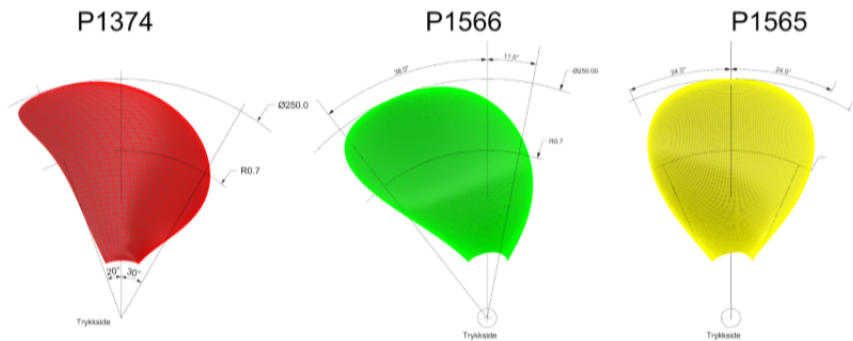


**Figure 3.4:** Outline of the Propeller Blades

was there shown that the relative location of the blade elastic axis and center of pressure had a significant influence on the deformation and resulting performance.

As the three propellers each has a distinct skew distribution, it was expected that changes in performance would occur. It should therefore be possible to assess the skew distributions influence on the hydroelastic behaviour.

### 3.2.2 Manufacturing of the Propellers

For each propeller geometry, a flexible propeller and a rigid propeller have been manufactured. The flexible propellers are labelled with AR, and the rigid propellers are labelled with AA.

The rigid propellers are made by aluminium alloy. Aluminium is flexible, but Savio & Koushan (2019) claimed that the elasticity of aluminium for use in model scale can be neglected, as their stiffness makes any deformations too small to observe. The flexible propellers are produced by resin casting with an epoxy resin and are isotropic. Resin material clearly shows deformations when loaded. This technology was chosen as it was rather cheap with a reasonably short production time for this specific case. The resin casting technique used silicon molds obtained by applying the metallic propellers as templates, and the specific resin was left to cure in a vacuum chamber with constant temperature. The Young's modulus of the resin is 2.15 GPa, which was the highest offered by the producer. That is relatively low, and a higher elastic modulus would be preferable to avoid viscoelastic effects.

More information regarding these propellers can be found in Savio & Koushan (2019).

### 3.2.3 Viscoelastic Effects

As stated, the propellers have a low Young modulus and viscoelasticity could therefore occur. These effects are an important consideration for model testing of flexible propellers. The effects can occur for the combination of high loading and low stiffness of the material. Viscoelasticity is, as explained by Papanicolaou & Zaoutsos (2011), the material property which exhibits a combination of elastic and viscous characteristics when undergoing deformation. Viscous deformation is time-dependent and the material will remain in the deformed state after unloading. Elastic materials deform instantaneously and return to its original state after unloading. Viscoelastic materials exhibit time-dependent strain, and a possible consequence of this effect is permanent deformation upon complete unloading of material. Figure 3.5 illustrate the possible permanent deformation upon complete unloading of the material.

For these propellers, the viscoelastic effects must be considered when deciding the operation conditions. The maximum hydrodynamic loading on the propeller

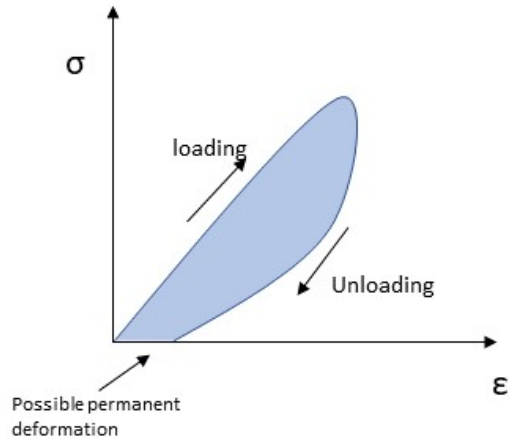


**Figure 3.5:** Viscoelastic Deformation

should be considerably lower than the tensile strength.

# Thruster Design

## 4.1 Azimuth Propulsion

The following section is based on research presented by Amini (2011) and Carlton (1994).

For an azimuth propulsion unit, the propeller can be rotated around the vertical axis and provides both propulsion and steering functions. The term azimuth propulsion unit includes both azimuthing thrusters and podded propulsors. Podded propulsors have an electric driven motor integrated in the thruster unit which is directly coupled with the propeller. Azimuthing thrusters have the propulsor powering machinery located in the ship hull and the propeller is driven through shafts and bevel gears.

Azimuth propulsion units are divided in pulling and pushing units. For a pulling unit, the propeller is located upstream of the pod housing and for a pushing unit, the propeller is located downstream of the pod. The different configurations are shown in figure 4.1. For a pulling unit, the propeller works in a more uniform wake, as the flow is not disturbed by the presence of the pod. This allows for a higher propeller loading. The pulling units will therefore generally have a higher efficiency, even though the drag of the propulsion unit increases due to higher propeller slip stream velocity. Pulling units require higher steering gear torques, as the steering gears work against the thruster turning the propeller downstream. Pulling and pushing azimuth propulsion units with one propeller are the most common configurations. There are also contra-rotating propellers and tandem propellers

which have one propeller in each end.

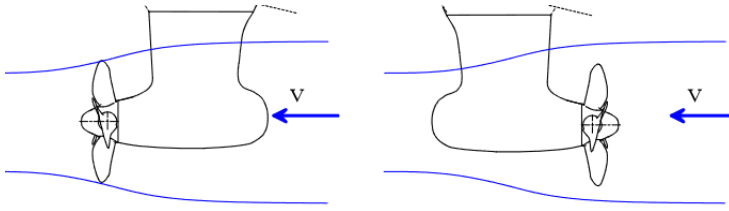


**Figure 4.1:** Pushing and Pulling Configuration-Picture taken from Steen (2014a)

Azimuth propulsion units have gained importance due to their dynamic positioning and manoeuvring capabilities. There is potential to improve the cavitation properties, to reduce vibration, noise and the fuel consumption compared to a conventional ship propeller. Use of azimuth propulsion units increases the flexibility in the ship and ship hull design.

However, the pod unit will increase the drag forces, and unexpectedly large hydrodynamic forces can occur on the unit causing mechanical failure problems. A combination of multiple installed propulsion units can have mutual interference that have significant effects on the behaviour of the ship, specially with regards to ship vibration. The extrapolation of model scale thruster is difficult, due to scale effects from the drag due to vortex generation and flow separation occurring on the pod.

#### 4.1.1 Literature Review for Azimuth Propulsion Units

Several publications have focused on azimuth propulsion units and their performance in different conditions. Research have been done both numerical and experimental. The mechanical response of an azimuth propulsion unit is different than for the conventional propeller. Amini et al. (2010) stated that the response to external excitation is altered due to the short and vertical shaft.

Islam et al. (2009) stated that the interaction between the pod unit, strut and propeller is complex, and the complexity increases in azimuthing conditions. Amini et al. (2010) investigated the thruster performance in different inflow conditions. It was observed that oblique inflows occurring for azimuthing conditions led to large shaft side forces and bending moments. Experiments done with a ventilated propeller or in waves had smaller side forces than in oblique inflows. At zero

azimuthing angle, Amini & Steen (2011) showed that the side force and bending moment in waves were considerably larger than for calm water. The publications mentioned that the ship hull would have a significant influence on the forces in waves, but it is likely that oblique inflows still lead to the largest forces. Amini & Steen (2011) did not include tests in extreme wave conditions in their study. It is important that resulting forces for all operation angles are evaluated to avoid mechanical failures.

The performance of a thruster unit in pulling and pushing configuration were evaluated by Islam et al. (2009). The unit thrust distribution was asymmetric for both configurations. For the pulling configuration, it was due to the interaction between wake and strut. For pushing configuration, both propeller and unit thrust performance were asymmetric due to difference in propeller inflow conditions. The force increased when the azimuthing angles coincided with the propeller rotation direction. The trend of the propeller torque was similar to that of the thrust. For all conditions, the puller configuration had larger forces than the pushing configuration. The pushing configuration had better steering forces than the pulling configuration due to the magnitude of the side force and steering moments. Amini et al. (2010) also observed larger side forces for pulling propulsor than pushing. Amini & Steen (2011) included the influence of the ship hull wake. A strong effect on the propeller performance and shaft bending loads were found when the propeller was turned outwards from the ship hull centreline.

Savio et al. (2011) performed CFD calculations on podded propellers. The interaction between the propeller and pod unit was the critical topic, and a possible reason for the large spread in numerical results compared to the experimental results. Amini et al. (2012) performed numerical calculations with different numerical methods and concluded that the side forces and bending moments were estimated with reasonable accuracy. The accuracy was heavily dependent on the numerical methods ability to capture the effective wake and viscosity.

## **4.2 Literature Regarding Thruster Design**

Some literature have presented optimization studies of the geometry of a thruster. Only information and conclusion relevant for puller configurations are presented.

The main dimensions of an azimuth propulsion unit are seen in figure 4.2.



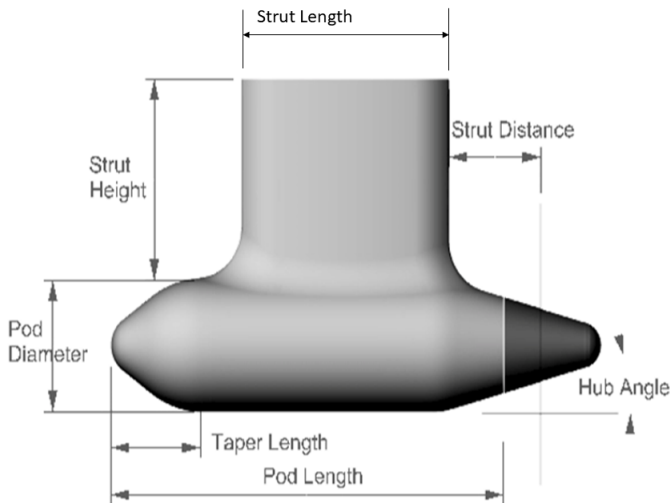


**Figure 4.2:** Thruster Dimensions, figure is modified from Molloy et al. (2006)

Islam (2009) investigated with an experimental study the effect of five geometrical parameters on the thrust, torque and efficiency of the propeller and unit of podded propulsors. 16 different pod-strut-propeller combinations were tested under similar conditions. It was observed that the pod diameter, hub angle and strut distance were the most significant parameters affecting the propulsive performance of the azimuth thruster. Variations in the pod length and taper length did not show any significant influence on the performance of the propulsors. Molloy et al. (2006) stated that a decrease in unit thrust was observed for longer pod lengths for the same experiments.

Islam (2009) claimed that an increase in pod diameter for a fixed propeller diameter led to increased propeller thrust coefficient and efficiency. A blockage effect of the pod was explained as the reason. Molloy et al. (2006) concluded however differently, that the propeller thrust coefficient increased for decreasing pod diameter, since a larger pod diameter meant higher drag on the pod.

An increase of strut distance had an opposite effect for short and long pod length values, as it led to an increase in thrust for short pod length value and a decrease for long pod length value.

As the hub angle increased, the thrust and efficiency increased for both pro-

PELLER and propulsors unit, and the effect was more pronounced at lower advance coefficients. Islam et al. (2008) concluded from the same experiments that an increase in the hub angle tended to decrease the maximum efficiency. The hub angle was seen to have a higher influence for pods with a high pod diameter.

Hoerner (1965) presented information on how the drag forces act on multiple types of submerged bodies. The relevant shapes with regards to thruster design are ellipsoidal bodies and aerofoil strut sections. For the streamlined aerofoil section, the skin-friction drag and pressure drag were seen to increase for increased thickness to chord ratio. The drag of ellipsoidal bodies was influenced by the ratio of the diameter to the length. For higher Reynolds numbers, little variation of the drag coefficient was observed.

### 4.3 Design of Thruster

The pod of the thruster unit was modelled in Rhinoceros and later 3D printed. It was fitted around the standard thrust body containing instrumentations and gears which are used by SINTEF Ocean when model testing thruster units. The dimensions of this standard model are presented in table 4.1. This standard model was the main limitation on the design of the podded thruster.

**Table 4.1:** Dimensions Limitations

<b>Pod diameter</b>	77.2 [mm]	<b>Taper length</b>	110 [mm]
<b>Pod length</b>	182.5 [mm]	<b>Hub diameter</b>	60 [mm]
<b>Strut distance</b>	43 [mm]	<b>Length to hub</b>	16 [mm]
<b>Strut diameter</b>	30 [mm]	<b>Gap distance</b>	2 [mm]

In addition to the limitations presented in table 4.1, it was required that the minimum thickness of the cap was 3 mm to ensure sufficient strength of the material. The model was 3D printed in two parts, and enough space had to be available to assemble the parts.

The dimensions were decided based on the literature from section 4.2. The objective was to maximize the unit efficiency at the design condition of the propulsion unit and minimize the drag forces on the unit. The minimum allowed pod length and pod diameter were decided, as a smaller pod unit simplified the manufacturing and less material should also lead to smaller drag forces. According to Molloy

et al. (2006) the thrust increased due to decreased drag forces for short pod diameter. For the strut shape, Hoerner (1965) showed how the drag increased with thickness to chord ratio. The strut shape was therefore decided to be slender, but simultaneously allowing for a sufficient strut distance. The pod unit is short, and Islam (2009) showed how a larger strut distance then would increase the thrust. Molloy et al. (2006) explained how the influence of the hub angle was more pronounced for larger units at low advance ratios. Due to the small size of the unit, the hub angle was not believed to have significant influence on the performance. This parameter was therefore decided based on the limitations from the standard thrust unit body. There is limited research on the influence of the taper length and its angle. It was mentioned by Islam et al. (2008) that the taper length did not have a significant influence on the performance. As mentioned, the minimum possible pod length, and thus taper length, was chosen.

Implications that arose from to the thruster design are commented in section 4.3.2.

The form of the thruster is designed as a part of the master thesis. Details related to the assembling and experiment are designed by SINTEF Ocean.

### 4.3.1 FleksProp Open Geometry Thruster

The main parameters of the thruster are shown in table 4.2. The strut has a NACA0033 shape. The pod has taper angle of 26 degrees. The thruster have a puller configuration.

**Table 4.2:** Dimensions Thruster

<b>Pod length</b>	248 [mm]	<b>Hub diameter</b>	60 [mm]
<b>Pod diameter</b>	92 [mm]	<b>Strut distance</b>	41.5 [mm]
<b>Strut length</b>	109 [mm]	<b>Strut thickness</b>	36 [mm]

The Rhinoceros model of the thruster is seen in figure 4.3 and the 3D printed model is seen in figure 4.4.

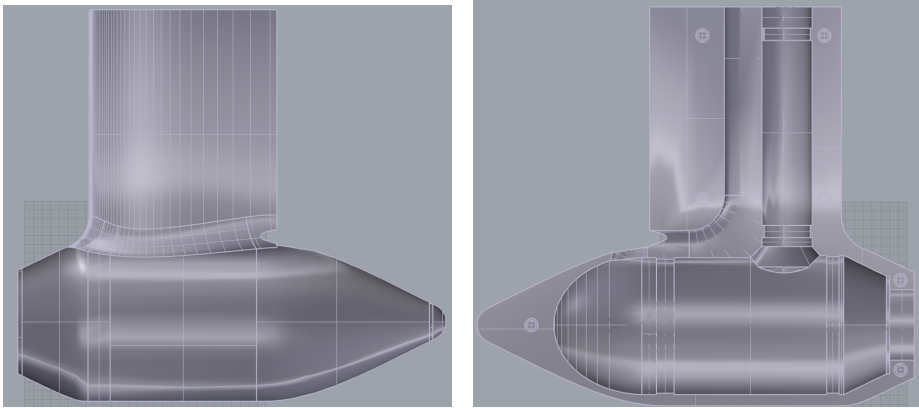


**Figure 4.3:** Thruster Unit Model Design in Rhinoceros

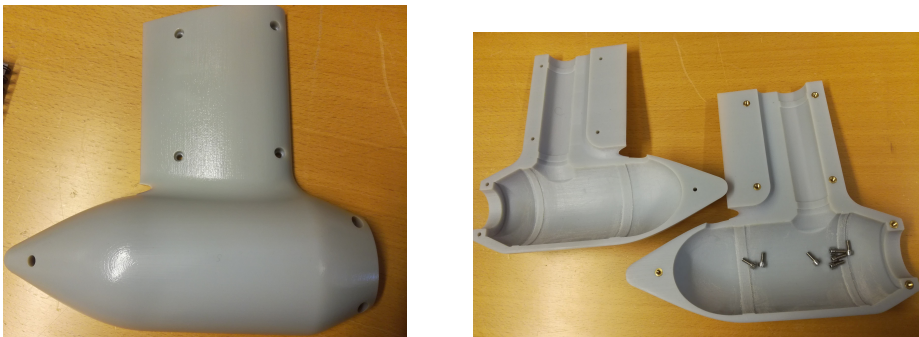


**Figure 4.4:** 3D Printed Version of the Thruster Unit

### **4.3.2 Comments Regarding Fleksprop Open Geometry Thruster**

Due to time limitations, this thruster unit design was not optimized and the performance was not controlled in advance by CFD calculations. Due to a relatively steep angle at the taper of the thruster, a flow separation can occur for lower velocities.

# Propulsion Unit Open Water Test

A series open water tests were carried out with the flexible propellers on a marine thruster in the beginning of March 2019 at SINTEF Ocean in Trondheim.

## 5.1 Open Water Test Procedure

The theory presented in this section is based on Carlton (1994) and Steen (2014a).

Propeller open water tests are conducted to determine the propeller characteristics without the presence of a ship hull. The test can be done in a cavitation tunnel or in a towing tank. The propeller rotational speed,  $n$ , is kept constant and the incoming velocity,  $V$ , is increased, and the propeller thrust,  $T$ , and propeller torque,  $Q$ , are measured. For azimuth propulsion, the entire thruster unit is tested in the open water test, and the total thrust of the unit is also measured.

The performance is presented non-dimensional in an open water diagram with the advance ratio  $J$ , eq. 5.1, the thrust coefficient  $K_T$ , eq. 5.2, torque coefficient  $K_Q$ , eq. 5.3, and efficiency  $\eta$ , 5.4.

$$J = \frac{V}{nD} \quad (5.1)$$

$$K_T = \frac{T}{\rho n^2 D^4} \quad (5.2)$$

$$K_Q = \frac{Q}{\rho n^2 D^5} \quad (5.3)$$

$$\eta = \frac{TV}{2\pi nQ} = \frac{J_A K_T}{2\pi K_Q} \quad (5.4)$$

Here, T is the thrust, Q is the torque, n is the rate of revolutions, V is the carriage speed and  $\rho$  is the water density.

For flexible propellers, the geometry changes for different loading conditions which will alter the propeller performance and thus the open water diagram. It is therefore possible to construct as many unique open water diagrams as loading conditions.

ITTC has recommended procedures and guidelines to perform open water tests to ensure consistency of methodology and acquisition of correct results for the different test facilities.

It is often necessary to extrapolate the results from the model tests to full scale. When extrapolating the results, the aim is to achieve geometric, kinematic and dynamic similarity between model and full scale. Geometric similarity means the structure have the same shape and deflection. Kinematic similarity means that velocities are geometrical similar. Dynamic similarity concerns the ratio between the forces. Typical scaling procedures are having an equal Reynolds number Rn, eq. 5.5, or Froude number Fn, eq. 5.6 in model and full scale. Reynolds number similarity scales the viscous forces correct and Froude number similarity scales the gravity forces. Reynolds number and Froude number similarity can not be satisfied at the same time.

$$Rn = \frac{VL}{\nu} \quad (5.5)$$

$$Fn = \frac{V}{\sqrt{gL}} \quad (5.6)$$

Here, is the characteristic velocity, L is the length,  $\nu$  is the kinematic viscosity and g is the gravitational constant.

In a hydrodynamic test facility, it is difficult to achieve Reynolds similarity as it leads to high velocities in model scale. For tests with a propeller, Froude similarity is only necessary if the free-surface effects must be taken into account. It is therefore common to perform the tests at a higher rotational speed than required by Froude similarity to make the scale effects viscous. This minimizes the flow separation and the extent of laminar flow on the propeller. The advance coefficient

J, eq. 5.1, must be equal in model and full scale. The cavitation number  $\sigma$  should be equal if cavitation is expected to arise.

Extrapolation of flexible propeller performance requires that the deformation is precisely scaled. The bend-twist coupling, thus propeller deformation, is influenced by the Young modulus  $E$ , shear modulus  $G$  and Poisson ratio  $\nu$ . The Poisson ratio should be kept equal in model and full scale. The ratios for the Young modulus and the shear modulus between model and full scale should be equal the scaling factor. This means the ratios are equal to the ratio between the lengths in model and full scale.

## 5.2 Experiment Set Up

The experiment was done in the towing tank and the propulsion unit was mounted on a towing carriage, displayed in figure 5.1. The towing tank dimensions are presented in table 5.1.

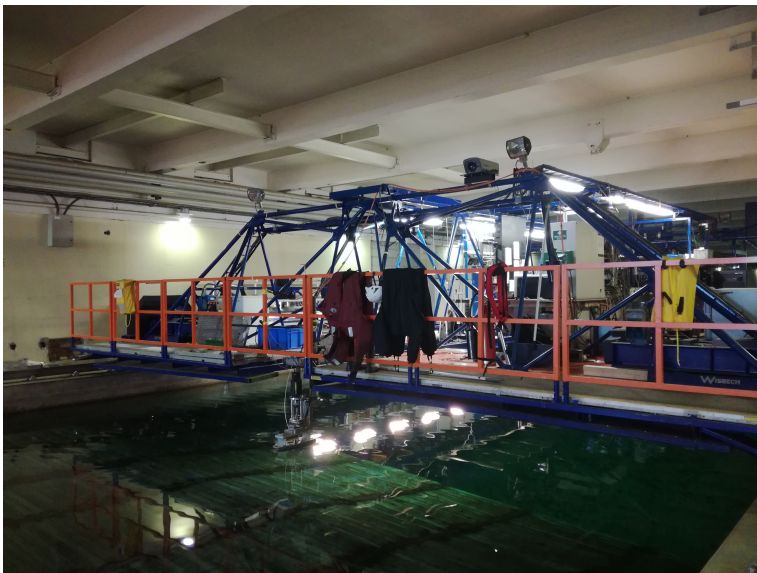


**Figure 5.1:** Carriage with the Propulsion Unit in the Towing tank

**Table 5.1:** Dimensions Towing Tank

<b>Length</b>	260 [m]
<b>Width</b>	10.5 [m]
<b>Depth</b>	5.6/10 [m]
<b>Maximum Acceleration</b>	1.0 [m/s <sup>2</sup> ]
<b>Maximum Velocity</b>	10 [m/s]

The set up of the propulsion unit without the propeller is seen in figure 5.2.

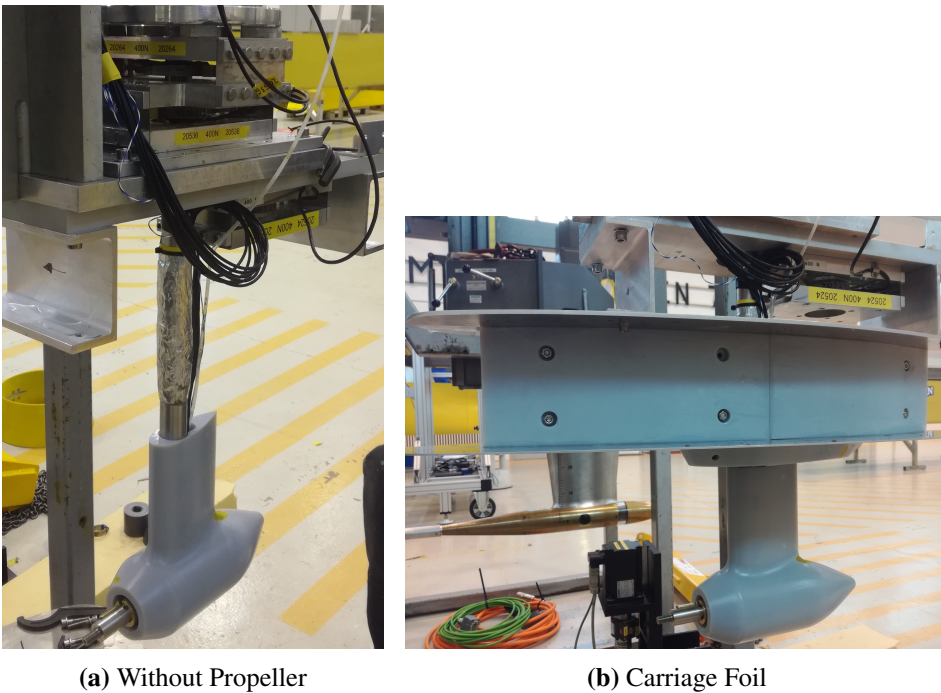


**Figure 5.2:** Set up of Propulsion Unit

The foil above the thruster, seen in figure 5.2, is used in model tests of propellers to minimize the wave formation. It reduced the waiting time between each run and minimized the impact from waves on the propeller. Two steel plates were attached to the foil. They are clearer shown in figure 5.4. The steel plate underneath the foil prevented ventilation of the propeller. The steel plate above prevented water splash on the instrumentations. The set up included a headbox, which



had no functions in model scale. For full scale, it acts as the structural foundation to ensure sufficient strength of the unit.

The measurement units were fitted in the standard thruster body from SINTEF Ocean as explained in section 4.3. The pressure within this body was controlled by an air hose, thus preventing water entry.

The thruster was 3D printed in two parts and attached together by small screws. The surface was later smoothen.

The same thruster unit and hub were used for all runs. The propeller hub had a half sphere shape with a length of 50 mm. Each propeller had their own propeller bearing, to shorten the necessary time to change propeller. Each bearing had a cylindrical shape with length 50 mm.

The set up with the propeller is seen in figure 5.3. In this figure, propeller P1374 made of aluminium was mounted on the thruster unit.

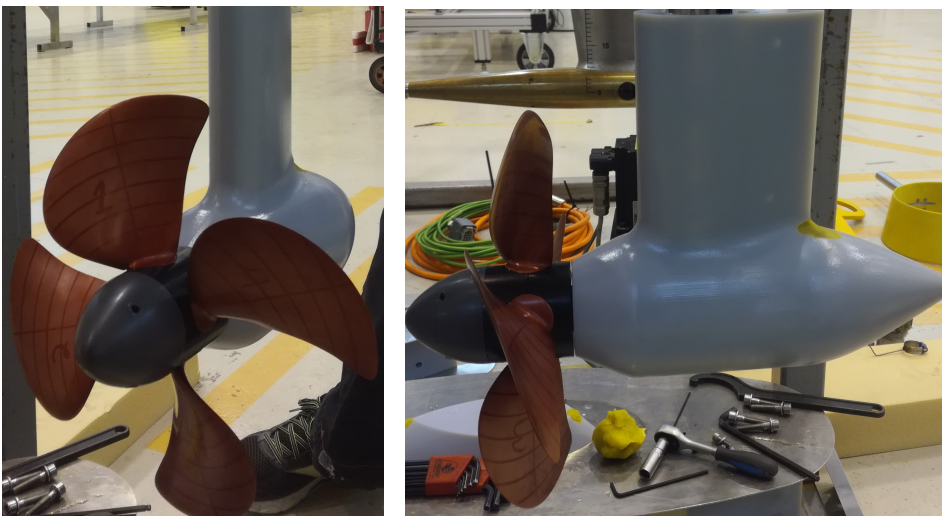


**Figure 5.3:** Thruster Unit with Propeller P1374AA

The digital drawing of the propulsion unit set up is seen in figure 5.4.

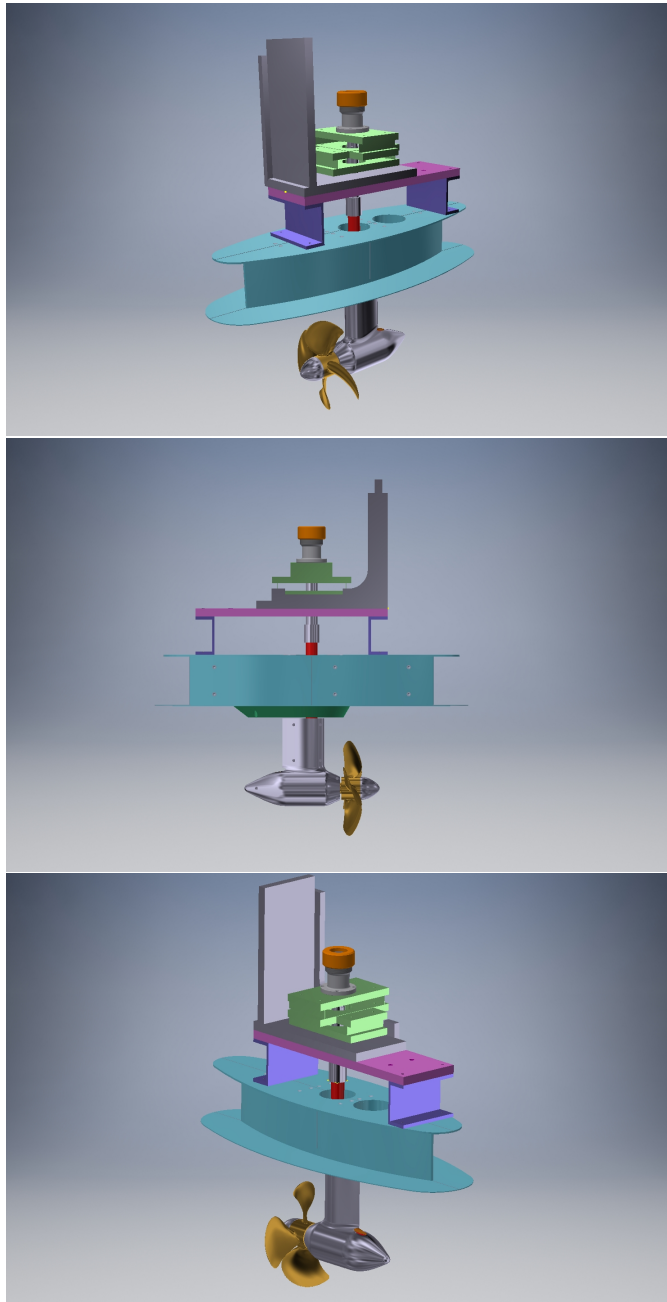


**Figure 5.4:** Digital Set up of Propulsion Unit

### 5.2.1 Measurements

An overview of all measurement channels is found in the appendix, section 7.3.

The propeller thrust,  $P_{\text{thrust}}$ , and torque,  $P_{\text{torque}}$ , were measured by a two component unit based on strain gauges at the propeller shaft. This dynamometer was calibrated against known weights before the experiment.

In the vertical shaft, there was a three component unit that measured the total forces in x- and y-directions and the moment around the z axis. The strain gauges can be seen in figure 5.2. These channels are named  $F_{x\_v\text{shaft}}$ ,  $F_{y\_v\text{shaft}}$  and  $M_{z\_v\text{shaft}}$ . The strain gauges were matrix calibrated ahead of the experiment. After the model test, doubts arose to these strain gauges, questioning if they accurately captured the forces aligned with the propeller axis. It has not been verified that a misdoing occurred, and the measurement channels were used to evaluate the performance.

The total thrust of the unit was also measured by two separate strain gauges on top of the unit, seen in figure 5.4. The shear forces in x- and y-direction were measured. These channels are named  $T_{\text{thrust}}$  and  $F_{y\_Total}$ . The strain gauges were calibrated against known weights. The strain gauge in the y-direction was calibrated after the experiment. As this unit was assumed stable, it was presumed that this would not affect the result. It later arose scepticism to the results from this strain gauge, and it was decided to neglect all the results from measurement channel  $F_{y\_total}$ .

The propeller rotational speed,  $P_{\text{rev}}$ , was measured by an encoder on the thruster shaft. The gear ratio between the propeller shaft and the thruster shaft is 12 to 23 and the same relation was used in the encoder for the measurements.

The carriage speed was measured by an encoder on the wheel of the carriage, called Speed in the channel list. It is calibrated on a regular basis by the towing tank personnel.

The water temperature was measured continuously during the runs by a thermocouple. As the changes in temperature and temperature gradients were negligible, the water temperature from the first measurement was used for all calculations.

## 5.2.2 Experiment Procedure

Hammer tests were done for each propeller to determine the eigenfrequencies of the propulsion unit. The propeller was excited, and the responding forces of the propeller were measured. The hammer test was done straight ahead on the propeller blade and on the hub, from behind on the unit and sideways on the propeller blade and thruster unit.

Each propeller was tested with the azimuthing angles  $0^\circ$  and  $\pm 10^\circ$ . The azimuthing angles were changed by moving the shaft of the thrust unit without changing the direction of the foil. Reference angle can be seen in figure 5.5.



**Figure 5.5:** Set Up Seen from Above

The propellers were tested with propeller rotational speed at 7 rps and 12 rps. These speeds were decided based on the open water tests previously done on the propeller, making it possible to compare the results. These rotational speeds should be unaffected by the eigenfrequencies of the unit, which were found from the hammer tests. The eigenfrequencies were around 10 Hz, and the response at propeller rotational speed 7 rps and 12 rps should not be significantly altered.

Each run had a constant rotational speed, and the carriage speed was increased. At each advance ratio, the carriage speed was kept constant for approximately ten seconds. The operational conditions of the propellers are shown in table 5.2. In addition, a bollard pull was done after the run to check if the propeller regained its

original shape after the run and avoided viscoelastic effects.

**Table 5.2:** Operational Conditions

V		
J/n	7 rps	12 rps
<b>0</b>	0.00 [m/s]	0.00 [m/s]
<b>0.2</b>	0.35 [m/s]	0.60 [m/s]
<b>0.4</b>	0.70 [m/s]	1.20 [m/s]
<b>0.6</b>	1.05 [m/s]	1.80 [m/s]
<b>0.8</b>	1.40 [m/s]	2.40 [m/s]
<b>1.0</b>	1.75 [m/s]	3.00 [m/s]
<b>1.2</b>	2.10 [m/s]	3.60 [m/s]

The resin propellers were tested three times at each operational condition and the aluminium propeller once. Three repetitions of the flexible propeller were done to evaluate the repeatability of the tests in case the propeller blades were permanently deformed during the runs. The runs were conducted with approximately 15 minutes inbetween to ensure that the water had calmed down.

Propeller P1374 in aluminium was tested first, before both versions of propeller P1566 and P1565 were tested. Propeller P1374 in resin was tested last. When mounting the last propeller, it was noticed that the shaft was not strictly fixed. This occurred after the first propeller was mounted, but a more exact time is unknown. It was not possible to see when it occurred or in which degree it affected the experiments when evaluating the propeller performance and harmonics.

The run matrix is seen in appendix 7.4.

### 5.2.3 Data Acquisition

Theory presented in this section is based on Steen (2014*b*).

The sampling frequency of the force measurements was 9600 Hz, and the sampling frequency of the carriage speed and propeller rotational speed was 200 Hz. The sampling frequencies of each measurements channel are shown in the appendix, section 7.3.

The Nyquist frequency, eq. 5.7, is the highest frequency that can be determined from the signal.

$$f_C = \frac{1}{2h} \quad (5.7)$$

$1/h$  is the sampling frequency.

If the signal contained frequencies that are higher than the Nyquist frequency, they would be folded back into the spectrum, appearing as non-physical components. This was avoided by applying an analog low-pass filter which removed all higher frequencies before sampling the signal. The cut-off frequencies of the low-pass filter were 20 Hz and 1000 Hz, around 1/10 of the sampling frequency.

The applied real-time low-pass filter could cause a time-delay due to a phase shift of the frequency. The phase shift is larger for higher frequency, and negligible for lower. The point where the phase shift turned significant is unknown for these model tests. The cut-off frequencies were therefore chosen sufficiently high, so that the frequencies of importance should not have been affected by the time lag.

The transducers were based on strain gauge and produced an analog output signal, which had to be digitized. An analog to digital (AD) converter performed this process of digitization. The range of an AD-converter should accept all input values, so that invalid values that disrupts the measurements will not occur. The resolution of the AD-converter is related to the number of bits used to represent a sample and could also introduce an error in the measurements. For these model tests, a resolution of 21 bits was used, which is believed to be sufficient to accurately represent the measurements.

The accuracy of the tests was dependent on the duration of each condition. A test should be sufficiently long to have established a steady-state response. In this experiment, the condition at each carriage velocity was measured for approximately ten seconds. This should have been sufficient to establish steady-state response, but deviation may occur at the highest carriage speeds.

#### **5.2.4 Processing of the Results**

The measurements were processed digitally to evaluate the performance and the vibrations associated with the propellers.

The steady state periods of the signals were established by defining a minimum time period where the rate of variations of a monitored channel should be less than a defined threshold value. The region was then considered as stable. Figure 5.6

highlights the steady state periods to the carriage speed for propeller P1374AR at propeller rotational speed 12 rps at zero heading angle. The mean values of all measurement channels were calculated for each steady state period.

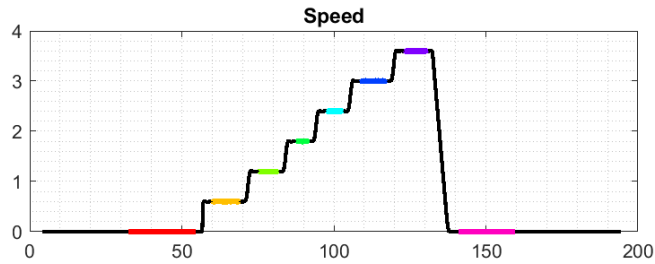


**Figure 5.6:** Stable Regions of the Speed for P1374AR

The mean values were used to evaluate the propeller performance using the procedure presented in section 5.1.

The spectra and harmonic responses of the propellers were found for each steady state period. Harmonics were found for the propeller thrust and unit thrust in both directions. The force time series for each steady state period were analyzed. The forces were from the measurement channels propeller thrust, P\_thrust, and propulsion unit thrusts in the vertical shaft, Fx\_vshaft and Fy\_vshaft. These channels had reliable results throughout the time series. The response amplitude operators, RAOs, for each propeller were found by the hammer test. The RAO for Fx\_shaft used the hammer test from behind the thruster, the RAO for FY used the hammer test sidewise on the thruster. For the propeller thrust, the hammer test on the hub was used. Figure 5.7 shows the RAOs of propeller P1374 for Fx\_vshaft and P\_thrust for aluminium and resin propeller.

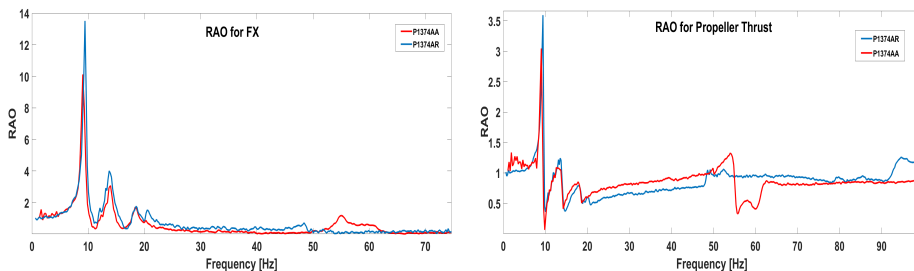


**Figure 5.7:** RAOs for P1374AA and P1374AR

The RAOs were used to apply a response filter on the time series. In addition, a lowpass filter was applied to remove frequencies higher than a defined value. The spectrum of the time series was found by a fast Fourier transformation. A defined number of harmonics were calculated based on the spectrum and the blade frequency. The blade frequency is the propeller rotational speed multiplied with the number of propeller blades. The response amplitude at each harmonic frequency was found. In addition, a range of  $\pm 0.5$  Hz was evaluated in case the energy from the propeller has been shifted to nearby frequencies. The total energy in this range was also used to calculate the response. A spectrum and the harmonic response were also found for the unfiltered time series following the same approach.



# Results

Parameters and coefficients used in this section are explained in the appendix 7.5.

## 6.1 Evaluation of Possible Viscoelastic Effects

The resin propellers can experience viscoelastic effects as explained in section 3.2. This could deform the propeller after the run and change the propeller performance.

To assess if the geometry regained its original shape, the bollard pull condition was measured after and compared to the bollard pull ahead of the run. Due to wave formation, the bollard condition after the run could have experienced ventilation. A comparison was therefore also done with the first bollard pull condition of the successive, repeating run.

The change in percentage between the bollard pull conditions was calculated for several runs following equation 6.2. For comparison, the percentage change was also calculated for the rigid propeller, despite that no deformation for these propellers was expected.

$$\mathbf{Difference} = \text{Last run} - \text{First run} \tag{6.1}$$

$$\mathbf{Percentage} = \frac{\text{Difference} * 100}{\text{First run}} \tag{6.2}$$

Table 6.1 presents the value and percentage of difference for propeller P1566AA

and P1566AR at 12 rps at zero heading angle. No repeating tests were done for the aluminium propellers, and the deviation is therefore only before and after each run.

**Table 6.1:** Changes in Bollard Condition for P1566

	$F_{ytotal}$	$T_{thrust}$	$P_{thrust}$	$P_{torque}$	$F_{xvshaft}$	$F_{yvshaft}$	$M_{zvshaft}$
<b>P1566AR</b>							
Before and after run							
<b>Deviation</b>	1.104 [N]	0.905 [N]	0.724 [N]	0.008 [Nm]	1.044 [N]	1.5458 [N]	0.097 [Nm]
<b>Percentage</b>	3.801 %	0.252 %	0.1923 %	0.057 %	0.279 %	77.37 %	1.13 %
Successive runs							
<b>Deviation</b>	0.689 [N]	-0.305 [N]	-0.626 [N]	-0.036 [Nm]	-1.501 [N]	0.079 [N]	0.145 [Nm]
<b>Percentage</b>	2.285 %	-0.085 %	-0.166 %	-0.246 %	-0.401 %	2.215 %	1.667 %
<b>P1566AA</b>							
Before and after run							
<b>Deviation</b>	1.355 [N]	0.117 [N]	0.639 [N]	0.044 [Nm]	0.544 [N]	0.526 [N]	-0.089 [Nm]
<b>Percentage</b>	4.421 %	0.036 %	0.186 %	0.351 %	0.162 %	21.721 %	-1.233 %

The results from these runs are representative for the experiment.

Changes between the runs were observed, but they were small in absolute value. In general, it was arbitrary if there was an increase or decrease. Large percentage changes were identified for the forces in y-direction. As the absolute value of the changes were small and close to negligible, it was concluded that these changes should be overlooked. The changes for the aluminium propeller were similar those of the resin propeller. Therefore, it was concluded that the material regained its shape after the runs, increasing the credibility of the propeller performance.

## 6.2 Propeller Performance

The propeller performance is presented by the thrust coefficient,  $K_T$ , torque coefficient,  $K_Q$ , and efficiency,  $\eta$ , as explained in section 5.1. The averaged thrust and torque of each steady state periods have been used.

For these model tests, three different thrust forces were measured. The propulsion unit thrust was measured by two separate strain gauges, one at the vertical shaft,  $F_{xvshaft}$ , and one above the setup,  $T_{thruster}$ . These measurements channels should have measured the same force. Both were used to evaluate the perfor-

mance. The propeller thrust force was also measured.

The Reynolds effect increases with the rotational speed of the propeller. It leads to higher thrust and torque. This effect could have been taken into account by evaluating the difference in performance of the aluminium propeller for different propeller speed. This has however not been done for these results.

### 6.2.1 Repeatability of the Propeller Performance

For the resin propellers, each condition was tested three times to check the repeatability of the runs. Figure 6.1 shows the open water curve for propeller P1374 made of resin for propeller rotational speed 7 rps at zero heading angle. The thrust coefficients of the three thrust measurements channels and the torque coefficients are included. The efficiencies based on propeller thrust and total unit thrust based on the T\_thruster are seen in the figure.

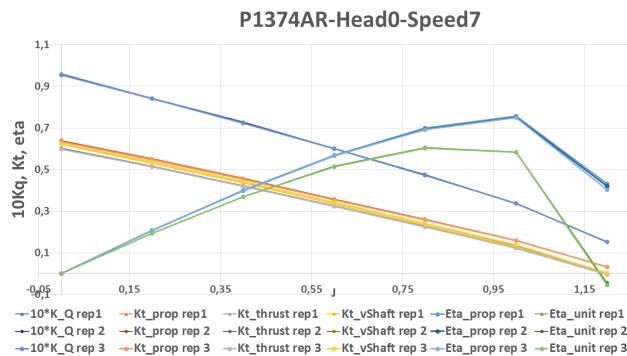


**Figure 6.1:** Open Water Diagram for Three Successive Runs for P1374AR

It is clearly shown in figure 6.1 that the runs repeated well when considering the propeller performance. This confirms the conclusion from section 6.1, that the material did not undergo any viscoelastic deformation and regained its original shape.

Based on this, it was decided to use the average thrust and torque coefficients when evaluating the propeller performance. The efficiencies were calculated with the average thrust and torque coefficients.

### 6.2.2 Open Water Curves

Open water curves have been made for each propeller rotational speed. The geometry of the flexible propeller changed with the loading condition, which led to unique open water curves. For the rigid propeller, the open water curves had been identical if the Reynolds effects were taken into account.

Open water curves have been made based on propeller thrust,  $P_{thrust}$ , and based on the total unit thrust,  $T_{thrust}$ .

Seven conditions were tested during each run. To have a smooth curve, a fifth degree interpolation has been applied. These results are displayed as lines in the open water curves. Data calculated directly from the measurements are shown in the diagrams as scatters.

The open water curves for all propellers are shown in figures 6.2, 6.3 and 6.4. Both the rigid and flexible propeller performance are included. Rigid propellers are titled with AA and flexible propellers are labelled with AR. The propellers operated with a propeller rotational speeds 12 rps in straight ahead condition.

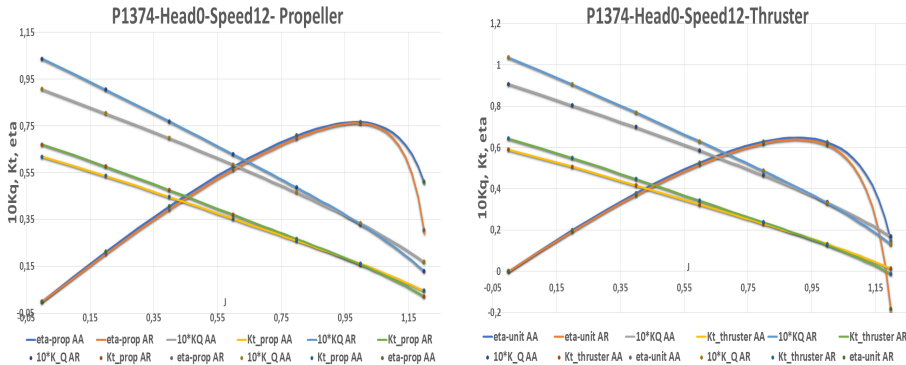


Figure 6.2: Open Water Diagrams for P1374

#### Comments to the Open Water Curves

Figures 6.2, 6.3 and 6.4 show a distinct difference in performance between the rigid and flexible propellers. The correspondence between the rigid and flexible propeller performance was best for P1566, the propeller with unbalanced skew, and worst for P1565, the propeller without skew.

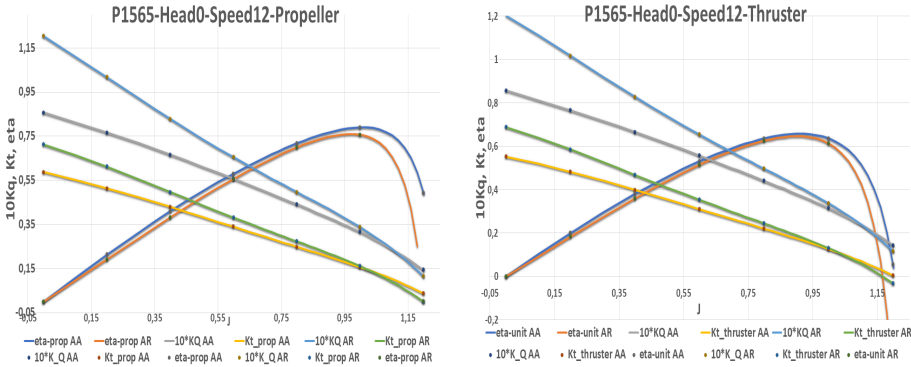


Figure 6.3: Open Water Diagrams for P1565

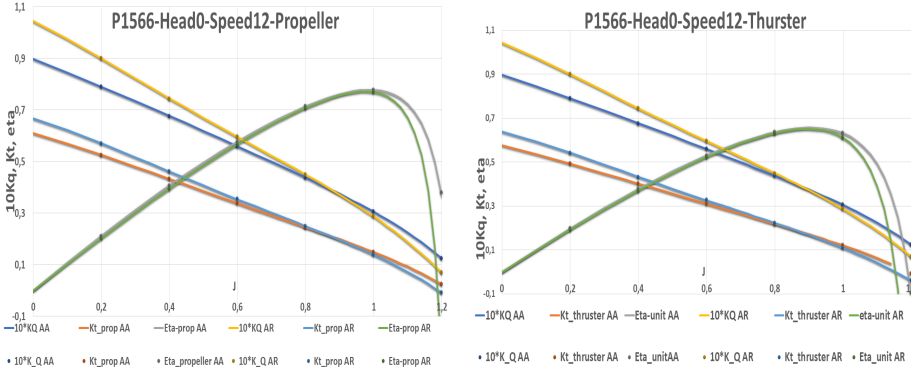


Figure 6.4: Open Water Diagrams for P1566

The performance of the rigid propellers were different, meaning that the skew distribution directly affected the propeller loading.

The flow induced twist increased for higher hydrodynamic loading according to Young et al. (2018). As the thrust and torque were higher for the flexible propellers, the twist had a nose-up direction. This means the center of pressure was upstream the elastic axis. The dependency of the center of pressure in relation to the elastic axis explain why the skew distribution affected the flow induced twist.

The efficiency is the most relevant propeller performance parameter. It was seen that the largest difference in efficiency occurred for high advance ratios, close to the maximum efficiency. The location of the maximum efficiency was similar for the different propellers. The propeller maximum efficiency occurred at around  $J=1.0$ , and the thruster unit efficiency occurred at around  $J=0.95$ . The propeller and

thruster unit efficiency were consistently worse for the flexible propeller compared to the rigid propeller. The maximum efficiency based on the propulsion unit was lower than that based on the propeller.

As mentioned, these propellers were not fabricated with an optimization of efficiency objective. An improvement in performance was therefore not expected.

### 6.2.3 Relative Difference Between Rigid and Flexible Propeller

The averaged performance of the rigid aluminium propeller compared to the that of the flexible resin propeller was evaluated by their relative difference. The relative difference between the rigid and average of flexible propeller is found by equation 6.3 and equation 6.4.

$$\Delta K_T = \frac{K_T^{rigid} - K_T^{flexible}}{K_T^{rigid}} * 100\% \quad (6.3)$$

$$\Delta K_Q = \frac{K_Q^{rigid} - K_Q^{flexible}}{K_Q^{rigid}} * 100\% \quad (6.4)$$

$K_T^{rigid}$  and  $K_Q^{rigid}$  are respectively the thrust and torque coefficient of the rigid aluminium propeller and  $K_T^{flexible}$  and  $K_Q^{flexible}$  those of the flexible resin propeller. A negative sign means that the parameter under consideration was larger for the flexible propeller.

Figures 6.5 and 6.6 show the relative difference for respectively the propulsion unit thrust coefficient and torque coefficient at propeller rotational speeds at 7 rps and 12 rps at zero heading angle. The results for rotational speed at 7 rps were scaled up to 12 rps using that the results are linear proportional to  $(12/7)^2$ . This can be done since the deformation is related to the load, which scales as the pressure coefficients, hence  $n^2$ .

The measurements were done for a wide range of advance ratios. For the highest advance ratios, due to the low absolute value of the forces, the results were sensitive to the measurement accuracy. These results have therefore been disregarded in the graphs. The graphs still represent the relative differences.

To simpler compare the performance of the propellers, figure 6.7 shows the relative difference in propeller thrust coefficient for all propellers at rotational speed

## 6.2 Propeller Performance

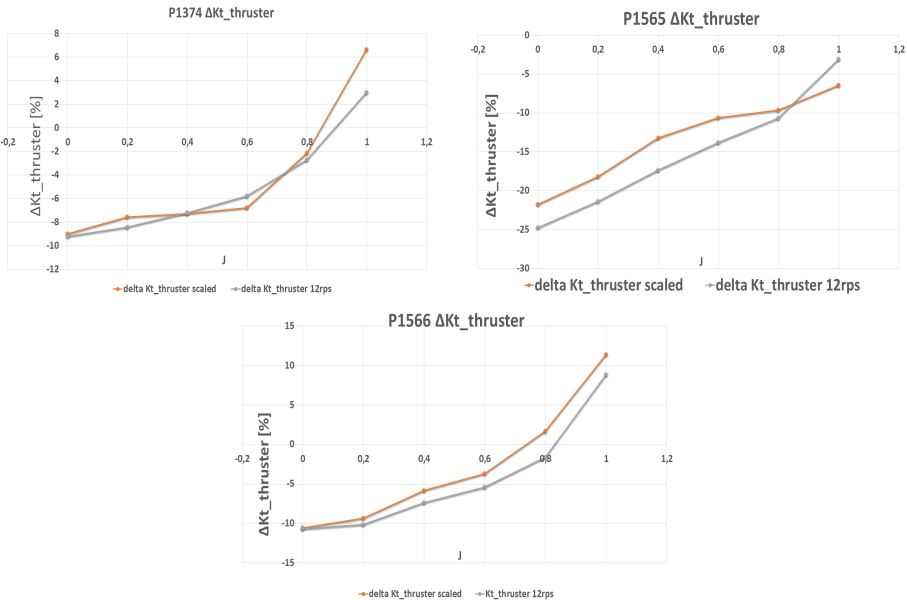


**Figure 6.5:** Relative Difference of Thruster Unit Thrust Coefficient in Straight Ahead Condition

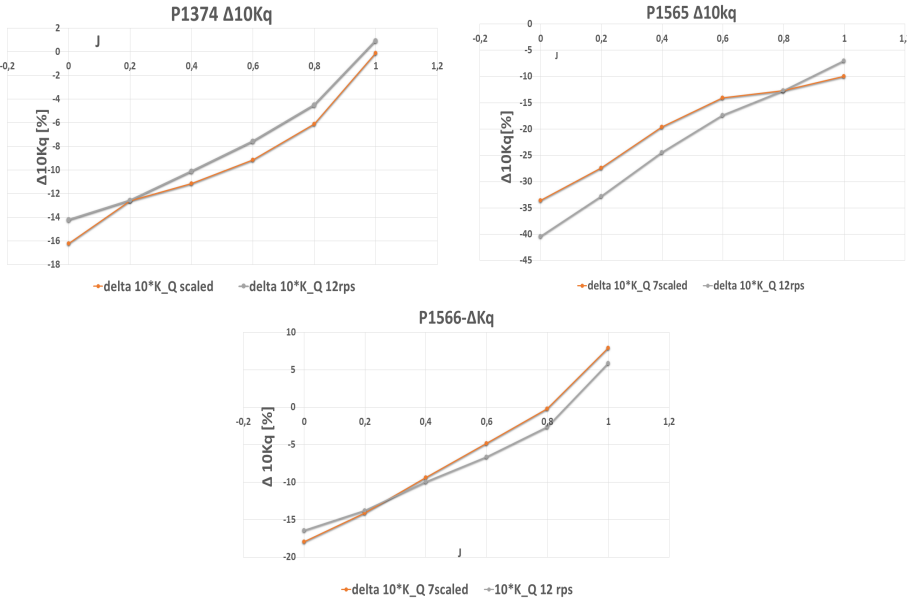


**Figure 6.6:** Relative Difference of Torque Coefficient in Straight Ahead Condition

12 rps at zero heading angle.

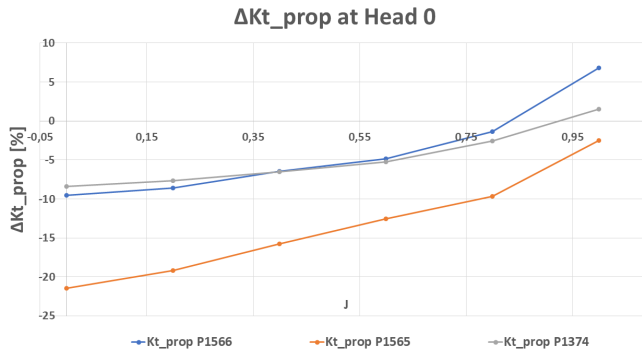


**Figure 6.7:** Relative Difference in Propeller Thrust Coefficient in Straight Ahead Condition

### Comments on the Relative Difference Between the Rigid and Flexible Propeller

The performance of the flexible propeller is dependent on the loading conditions as the propellers will constantly change its geometry. Therefore, these graphs are only valid for loading conditions corresponding to a propeller rotational speed of 12 rps.

The graphs in figure 6.5 and 6.6 include the results from both the runs at 12 rps and for 7 rps, scaled up to 12 rps. The Reynolds effect was higher for propeller rotational speed 12 rps, which increased the thrust and torque at this speed. This affected the comparability between the rotational speeds. However, the scaled results still showed a good correspondence with the results at 12 rps. This indicates that the rotational speeds led to a similar behaviour. It should therefore be possible to have a general conclusion for the flexible propellers behaviour in comparison with the rigid propellers.

The relative difference is defined so that it is positive when the rigid propeller coefficients are greater than those of the flexible propeller. At zero heading angle, the relative difference of the unit thrust, propeller thrust and torque coefficients were seen to follow a linear trend with the advance ratios. The relative difference was negative at low advance ratios and the largest deviation occurred for all



propellers at the lowest advance ratio. The coefficients of the flexible propellers decreased compared to those of the rigid propellers when the advance ratio increased. The relative differences in unit thrust and propeller thrust coefficients were similar. The relative difference in the torque coefficient at low advance ratios was for all propellers higher than those of the other coefficients.

Propeller P1565, which has zero skew, had the largest difference in both thrust and torque coefficients at low advance ratios. For isotropic materials, the bend-twist coupling occurs when the center of pressure is away from the elastic axis. The location of the pressure center and elastic axis of the propeller blade without skew would be significantly altered compared to those with skew. This could have led to the larger differences compared to the other propellers. For this propeller, the relative differences for all channels were negative for all advance ratios in straight ahead condition. This means that the rigid propeller consistently had lower thrust and torque.

At higher advance ratios, the difference between the rigid and flexible propeller was largest for propeller P1566, the propeller with an unbalanced skew distribution. The difference was largest for the unit thrust coefficient, and the rigid thrust coefficient was higher than that of the flexible propeller. Due to its skew distribution, this propeller has a blade tip which behaves differently. There is high centrifugal forces at the blade tip. Savio (2015) observed a backward bending of the blade tip when the load approached zero, which could be the reason for this behaviour.

### **6.2.4 Relative Difference For Varying Heading Angles**

The tests with the thruster unit were done for azimuthing angle  $0^\circ$  and  $\pm 10^\circ$ . When the thruster operated with a heading angle relative to the carriage motion, the measurements were done in different directions. The total unit measurement,  $T_{thrust}$ , was done in the direction of the carriage. The propeller thrust,  $P_{thrust}$ , and the vertical shaft measurements,  $F_{x\_vshaft}$  and  $F_{y\_vshaft}$ , were done in the direction of the propeller, and therefore changed direction with the heading angles. All results have been converted to the direction of the carriage.

For the forces measured in the vertical shaft, the contribution in the carriage direction was found using equation 6.5. This is possible since the forces in both x-

and y-directions were measured.

$$Fx_c = Fx_p \cos\theta - Fy_p \sin\theta \quad (6.5)$$

Subscript  $c$  represents the carriage reference system, and subscript  $p$  represents the propeller reference system. In the carriage reference system,  $Fx$  is the force component along the tank and  $Fy$  is the force component across the tank. The difference between carriage and propeller direction is shown in figure 6.8. The azimuthing angle is represented by  $\theta$ .

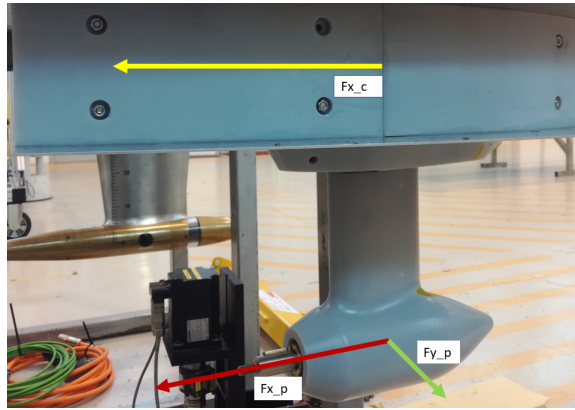


**Figure 6.8:** Force Directions

The propeller thrust was only measured in one direction. The trajectory in the carriage direction has been used in the calculation, which is shown in equation 6.6. Similar approach was used to find the influence of heading angles on the advance ratio, equation 6.7.

$$Fx_c = Fx_p \cos\theta \quad (6.6)$$

$$J_c = J_p \cos\theta \quad (6.7)$$

The relative difference between the average thrust coefficients of the rigid and flexible propeller, eq. 6.3, is used to evaluate the effect of the heading angle on the performance. The relative difference is positive when the rigid propeller coefficients are larger than the flexible propeller. Figure 6.9 shows the relative dif-

ference in propeller thrust coefficient of each propeller at azimuthing angle  $0^\circ$  and  $\pm 10^\circ$  with a rotational speed 12 rps. All parameters are in the direction of the carriage.

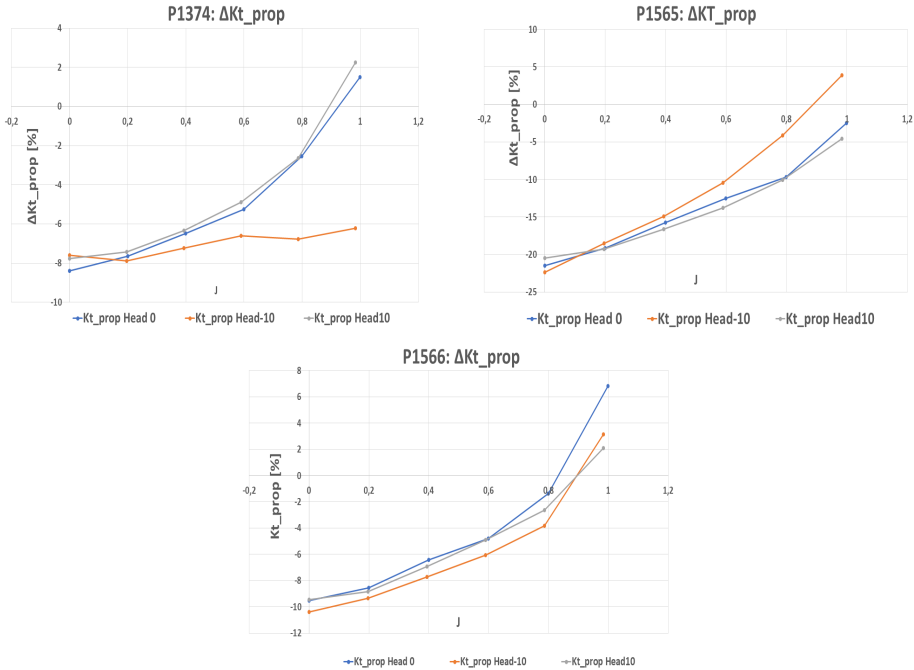


**Figure 6.9:** Comparison of Propeller Thrust Coefficient for Varying Heading Angles

The influence of the skew distribution for operation with azimuthing angles is shown in figure 6.10. The figure shows the relative difference in propulsion unit thrust coefficients based on the vertical shaft measurements,  $F_{x\_vshaft}$ , for all propellers at rotational speed 12 rps. The forces are in the carriage direction.

**Comments on the Relative Difference for Varying Heading Angles**

The heading angle was seen to have a significant influence on the performance, and the influence changed for different skew distributions. A heading angle led to oblique inflow of the propeller. This increased the complexity of the strut-pod-propeller interactions of a thruster unit, which is explained in section 4.1.1. The thrust coefficients are based on the averaged thrust, which suppresses some of the effects of this complexity.

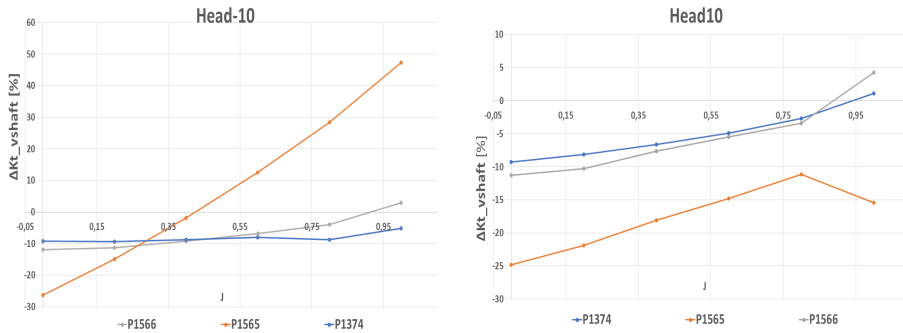


**Figure 6.10:** Relative Difference of Unit Thrust Coefficients for Azimuth Angles

Due to interactions between the thruster unit and the wake, the unit thrust distribution of a pulling unit is asymmetric. It was seen that the performance of the propellers was altered for heading angle  $-10^\circ$  compared to the two other directions. The propellers are right-handed, and the resulting velocities of the propellers was therefore significantly transformed in this condition. Islam et al. (2009) reported that the forces increased when the azimuthing angles coincided with the propeller rotation direction.

The performance of the propeller with balanced skew, P1374, at azimuthing angle  $-10^\circ$  was considerably altered for both propeller and unit thrust coefficient. Its relative difference of both unit and propeller thrust coefficients were approximately unchanged for increased advance ratios.

Propeller P1565 had the largest relative difference for both unit and propeller thrust coefficients for most conditions. At heading angle  $-10^\circ$  had the rigid propeller higher thrust than the flexible propeller. At this azimuthing condition, the propeller had a large relative difference for the unit thrust coefficient at high advance ratios. The largest difference between rigid and flexible propeller was around 40%, which is significant large. The previous section explained the difference between rigid and flexible thrust coefficient for this propeller.

It is notable that for propeller P1374 and P1565, the absolute value of the relative difference increased in azimuthing conditions. For propeller P1566, which has unbalanced skew, the difference between rigid and flexible propellers was smaller for azimuthing conditions at high advance ratios.

### 6.2.5 The Thruster Units Influence on the Performance

In 2018, open water tests with the propellers was done in the towing tank. The propellers were tested at rotational speeds 7 rps, 9 rps and 11 rps. Savio & Koushan (2019) presented this model test in detail.

To evaluate the effect of the thruster unit on the performance, the relative difference between propeller and propulsion unit performance has been calculated for the propeller thrust and torque coefficients, eq. 6.8 and eq. 6.9. The differences were calculated for both the aluminium and resin propellers.

$$\Delta K_T = \frac{K_T^{Propeller} - K_T^{Thruster}}{K_T^{Propeller}} * 100\% \quad (6.8)$$

$$\Delta K_Q = \frac{K_Q^{Propeller} - K_Q^{Thruster}}{K_Q^{Propeller}} * 100\% \quad (6.9)$$

Both  $K_T^{Propeller}$  and  $K_T^{Thruster}$  represent the propeller thrust coefficient.  $K_T^{Propeller}$  is the propeller thrust coefficient based on the propeller open water test.  $K_T^{Thruster}$  is the propeller thrust coefficient based on the propulsion unit open water test.

The relative differences between propeller thrust and torque coefficients for the propeller and propulsion unit open water performance are shown in figure 6.11. In the figure, both propellers operated at 7 rps in a straight ahead configuration. The difference in efficiency is included in the graph.

#### Comments on the Thruster Units Influence

The effect of the thruster unit on the performance was similar for the aluminium and the resin propellers. Larger discrepancies were observed for high advance ratios. Due to the small absolute values, this can be due to the sensitivity of the measurement equipment.

The thrust and torque coefficients were greater for the thruster unit at higher advance ratios. This was due to a blockage effect from the propulsion unit which reduced the effective incoming velocity to the propeller.

The difference in efficiency of the propeller for all conditions were close to zero. For an azimuth propulsion unit, it is the total thrust and corresponding thruster unit efficiency that are of importance for the power predictions. As shown

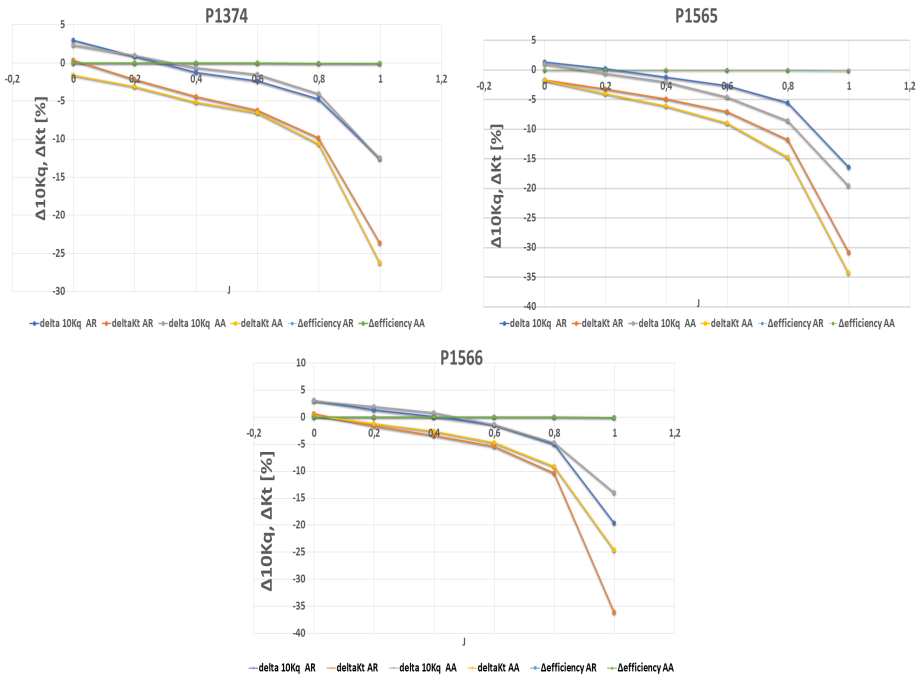


**Figure 6.11:** Difference in Performance for Propeller and Thruster Unit Open Water Tests

in section 6.2.2, the efficiency based on the thruster unit was lower than the propeller efficiency. The efficiency would therefore be greater when only a propeller is used.

### 6.3 Propeller Harmonics

Harmonics are periodic fluctuations or characteristics vibrational modes. The thrust and torque of the propulsion unit can be enhanced at the harmonics frequencies with an amplitude that fluctuates around a zero mean value. The harmonic frequencies are related to each other by whole number ratios. For marine propellers, the most prominent frequency is typically the first blade harmonic. This is defined as the propeller rotational speed multiplied with the number of blades.

The responses at the harmonic frequencies were evaluated for the time series of the propeller thrust and the vertical shaft thrust in x- and y-direction.

The response is given non-dimensional following equation 6.10. This means

that it is divided with the thrust coefficient of the propeller made of the same material at an advance ratio 0.8 in straight-ahead condition. The response for the  $Fy\_vshaft$  time series is divided with the thrust coefficient from  $Fx\_vshaft$ , and the two other measurement channels use their own thrust coefficients. The thrust coefficient is for the same propeller rotational speed.

$$Response[-] = \frac{\Delta K_T}{K_T(J = 0.8, Head = 0^\circ)} \quad (6.10)$$

The measurements for  $Fx\_vshaft$ ,  $Fy\_vshaft$  and  $P\_thrust$  were done in the direction of the propeller. The results from runs with a heading angle have been converted back to the carriage direction. The approach is explained in section 6.2.4.

The resin propellers were tested three times for each condition. If not stated otherwise, the measurements from the first run are used in the calculations.

### 6.3.1 Harmonic Response and Corresponding Spectrum

Initially, ten harmonic responses were calculated for each steady state period. It was seen that for higher harmonics, unexpected and high responses occurred for different propellers and measurements channels. The corresponding spectra were evaluated. Figure 6.12 shows the response and corresponding spectra for propeller P1374 made of resin at advance ratio 0.8 with rotational speed 7 rps and  $-10^\circ$  heading angle. The response is calculated at the exact harmonic frequencies.  $FX$  represents the harmonic response and spectrum for the vertical shaft thrust in  $x$ -direction,  $FY$  represents the thrust in  $y$ -direction and  $PT$  is the propeller thrust.

The main contributions to the energy in the spectrum were from the propeller frequency and from the gear. Those related to propeller frequencies correspond with the harmonic frequencies. The frequencies related to the gear correspond to the gear ratio, 23 to 12, multiplied with the propeller rotational speed and is linked by whole number ratios. In figure 6.12, the energy related to the gear is shown in magenta and the energy related to the propeller, and thus the harmonic frequencies, is shown in green.

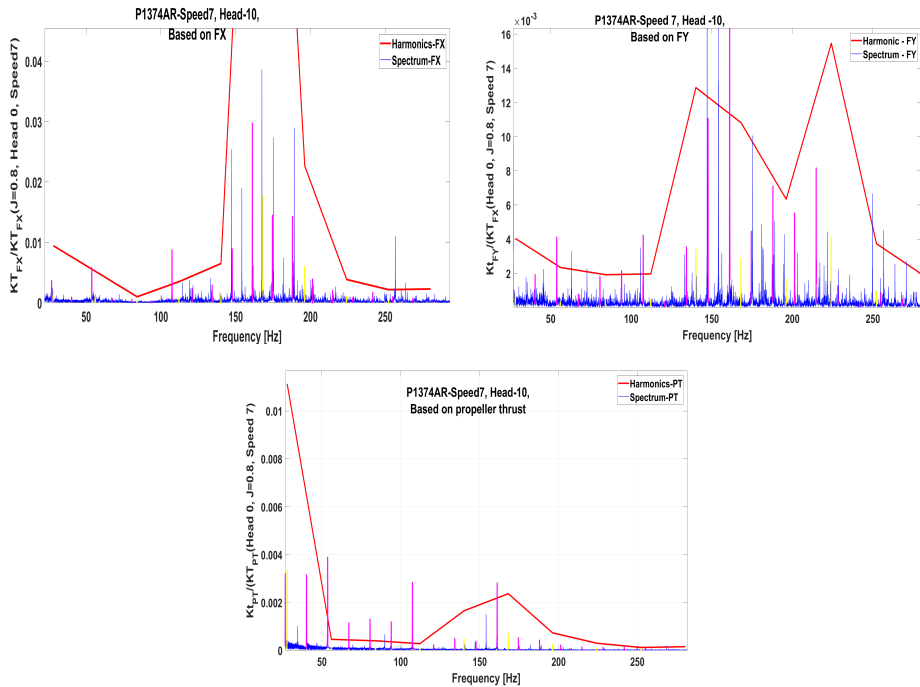


**Figure 6.12:** Harmonic Response and Corresponding Spectrum for P1374AR

### Comments Regarding the Spectra

A correspondence between the spectrum at the harmonic frequency, shown in green, and the dynamic response is seen. Nevertheless, it was seen that the response was high for several frequencies that were related to neither the propeller nor the gear.

The response for several propellers at rotational speed 7 rps at different heading angles were evaluated. Table 6.2 presents the frequencies related to the large peaks in the spectra which were not associated with the propeller or the gear. These peaks were either significantly larger than the other nearby amplitudes in the spectra or higher than a threshold value of 0.1 Hz.

Table 6.2 demonstrates that several of the same frequencies unrelated to the propeller rotational speed and the gear excited large responses regardless of the propeller and measurement channel. This suggests that these peaks were not related to the physics of the propellers, but the set up of the propulsion unit. They are therefore considered as noise. Based on table 6.2 and figure 6.12, it is decided



Frequency [Hz]	P1374AR-Head-10°	P1374AA-Head0°	P1565AR-Head0°	P1566AR-Head10°
81.67		Fx		
89.9	Pt	Pt	Pt	Pt
133.1	Fy		Fy	Fx
147.1	Fx, Fy	Fy	Fx	Fx, Fy
154.1	Fx, Fy, Pt	Fx, Fy, Pt	Fy, Pt	Fy, Pt
156.2		Fx		
175.1	Fx, Fy		Fx, Fy	Fx
180.9	Fy, Fx			Fx
189.1	Fx	Fx, Pt	Fx, Fy	Fx
256.9		Fy	Fy	Fy
263.9		Fy	Fy	

**Table 6.2:** Occurrences of Peaks in Spectra

that only the first four harmonics should be evaluated.

The harmonic response was calculated from the spectrum at the exact blade harmonic frequencies and for a range of  $\pm 0.5$  Hz of these frequencies. For the range  $\pm 0.5$  Hz, the energy in the range was conserved and used to calculate the response. As shown in figure 6.12, the spectrum contained noise, which could have affected the response when the range around the blade frequency was considered. Due to this, the harmonics were decided to be calculated with the exact blade harmonic frequencies. Some of the energy to the harmonics could have been slightly shifted to the nearby frequencies, and they are not captured by this approach. It is possible that some results still were affected by noise.

### 6.3.2 The Advance Ratios Influence on the Harmonics

The harmonics were calculated for each advance ratio.

Figure 6.13 shows the first four harmonics of different advance ratios for propeller P1566AR at propeller rotational speed 12 rps at 10° heading angle.

Figure 6.14 shows how the response of the first four harmonics changed with the advance ratios for propeller P1374AR. The propeller operated with rotational speed 7 rps at zero heading angle.

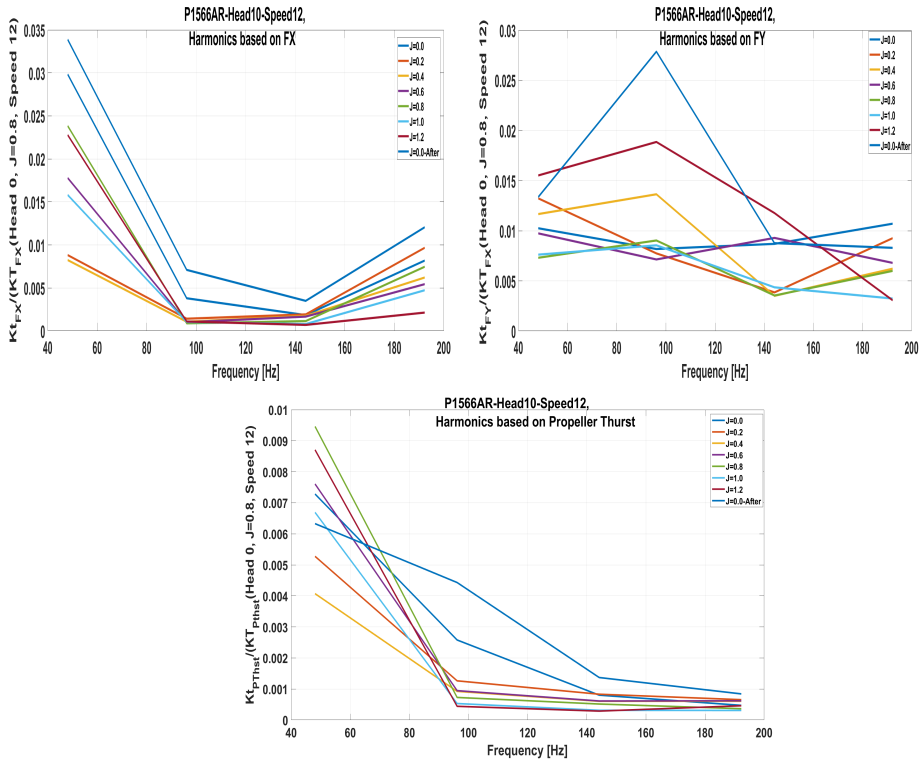


Figure 6.13: Harmonic Response of the Different Advance Ratios for P1566AR

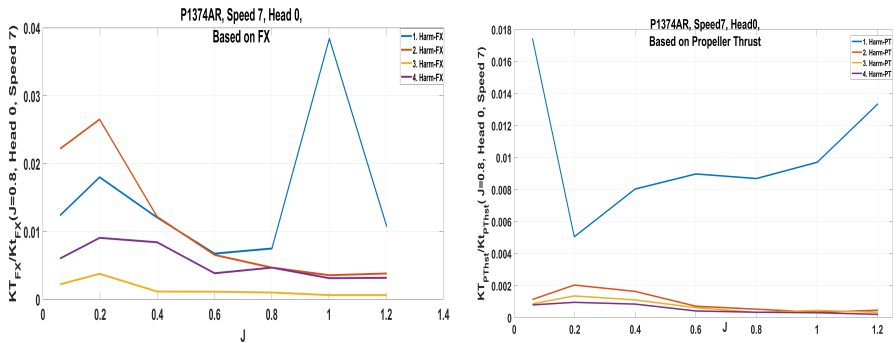


Figure 6.14: Harmonic Response for P1374AR with Changing Advance Ratios

### Comments on the Influence of Advance Ratio

Figure 6.13 and 6.14 show that the harmonic responses changed with the advance ratios. The greatest deviation between the responses was around 0.025, corre-

sponding to 2.5%, for the first blade frequency of P1566AR based on FX. At advance ratio  $J=0.0$  and  $J=1.2$ , the responses deviated more than for the rest of the sample. For advance ratios between 0.2 to 1.0, the responses were approximately constant.

When the response is shown for the first four harmonics, it was decided that advance ratio 0.8 should be used to represent the sample. This advance ratio was less sensitive to noise than the higher advance ratios, but is still in the range of the maximum efficiency. Nevertheless, care must be taken when using this approach, as variations with the advance ratio may occur.

### 6.3.3 The Harmonics of the Repeating Runs

For the flexible propellers, each condition was tested three times to review the repeatability of the results. Figure 6.15 shows the harmonic response for the repeating runs of propeller P1374AR at rotational speed 7 rps with advance ratio 0.8 in straight ahead condition.

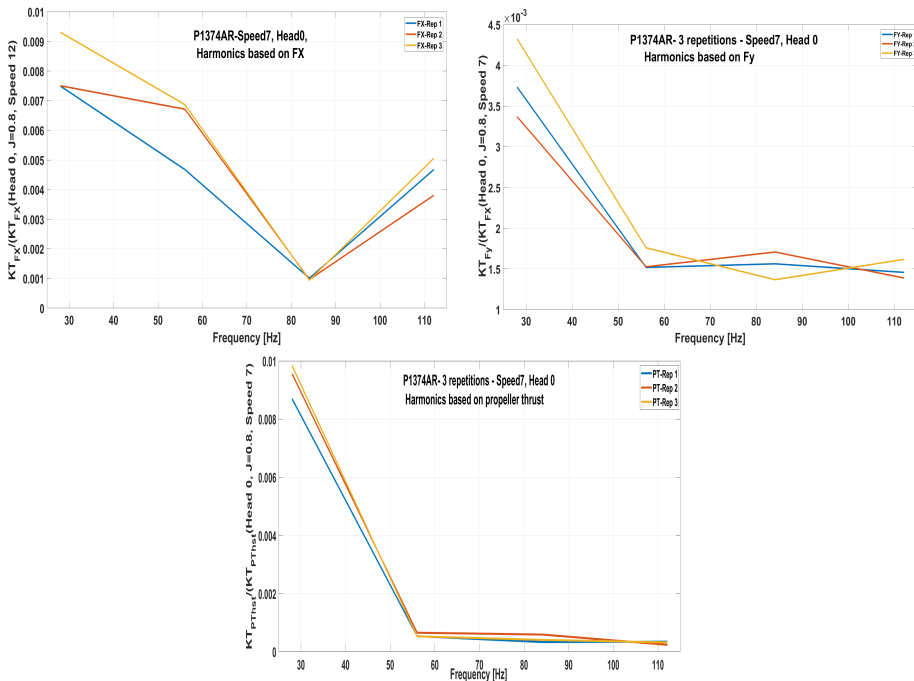


Figure 6.15: Harmonics for P1374AR for Repeating Runs

### Comments Regarding the Repeatability

Figure 6.15 shows that the deviation between the different runs was small. Largest difference occurred for the first harmonic of FX, for which there was around 0.2% difference between the first and last run. This can be considered as negligible. The results showed a good repeatability of the test which suggested that the propeller blades were not permanently deformed during the runs.

The repeatability can also be determined by the correspondence between the first and last bollard pull. These conditions should have similar results. The harmonic responses of propeller P1566 at different advance ratios are shown in figure 6.13. The responses for the different bollard pull conditions were similar. This amplifies the conclusion that the tests had a good repeatability and that the propeller blades regained its original shape.

Based on the results in figure 6.15, it was decided that the results for the first repetition will be used.

### 6.3.4 Harmonics for Both Propeller Rotational Speeds

The propellers operated with rotational speed 7 rps and 12 rps. Figure 6.16 shows the harmonics for propeller P1565AR in straight ahead condition for both rotational speeds with advance ratio 0.8. The corresponding frequencies for the run at 7 rps have been scaled up using the ratio between the rotational speeds, 12/7, to easier compare the results.

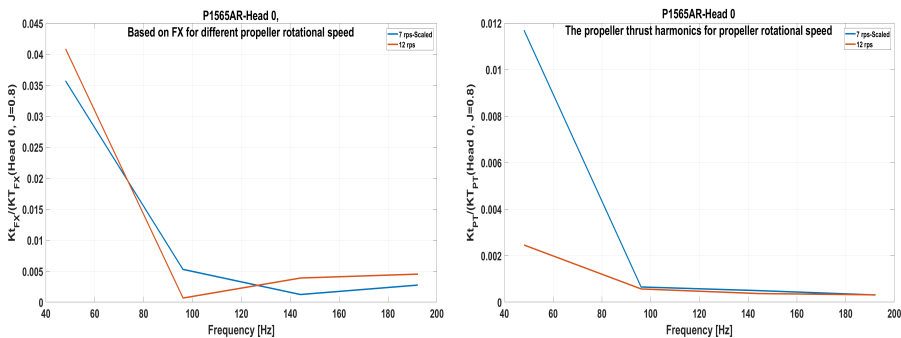


**Figure 6.16:** Harmonic Response for P1565AR at Speed 7 and 12 rps

Figure 6.17 shows the first harmonic response for propeller P1374AR for both

propeller speeds with the advance ratio in straight ahead condition.

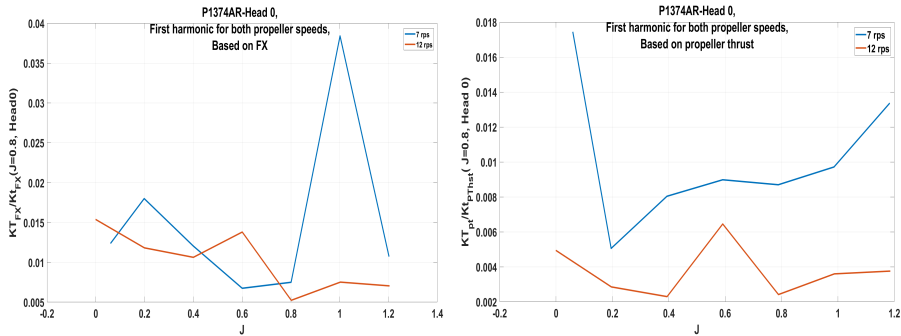


**Figure 6.17:** Harmonic Response for P1374AR at Speed 7 and 12 rps with Advance Ratios

### Comments on the Harmonics for Propeller Rotational Speeds

Based on figures 6.16 and 6.17 it is seen that the harmonics from propeller thrust changed with the propeller rotational speed. For the first harmonic, the response for propeller rotational speed 7 rps was higher than at 12 rps for all advance ratios. The largest difference was around 1%. The propeller thrust response at higher harmonics were seen to be negligible, and no difference between the rotational speeds was observed. The Reynolds effect leads to higher thrust, and it is higher for rotational speed 12 rps than 7 rps. The thrust coefficients, which were used to make the harmonics dimensionless, increased. It is possible that this resulted in the difference in response for the two rotational speeds.

It was not possible to observe a similar tendency for the harmonics based on  $F_{x\_vshaft}$ . For this measurement channel, it was arbitrary which propeller rotational speeds induced highest response as it changed with harmonics and advance ratio. The largest difference in the response occurred for propeller P1374AR at  $J=1.0$ , where the difference was around 4%. This was a large response, and it is possible that it has been influenced by noise.

### 6.3.5 Influence of Skew Angle on Harmonics

Figure 6.18 shows the first harmonics for all propellers in straight ahead condition at rotational speed 7 rps.

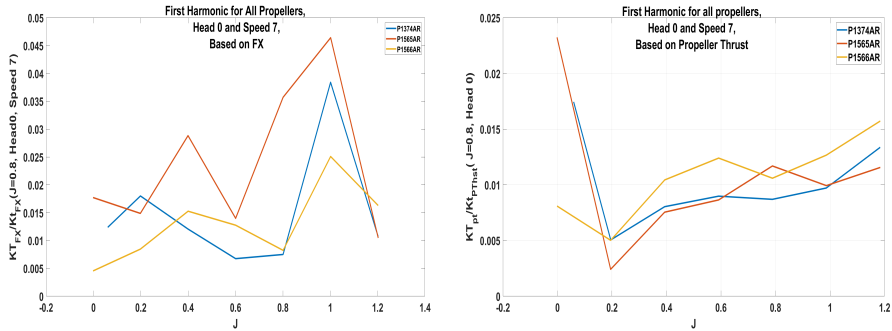


Figure 6.18: First Harmonic for all Propellers at Zero Heading

Figure 6.19 shows the harmonic response at advance ratio  $J=0.8$  in a straight ahead condition with propeller rotational speed 12 rps.

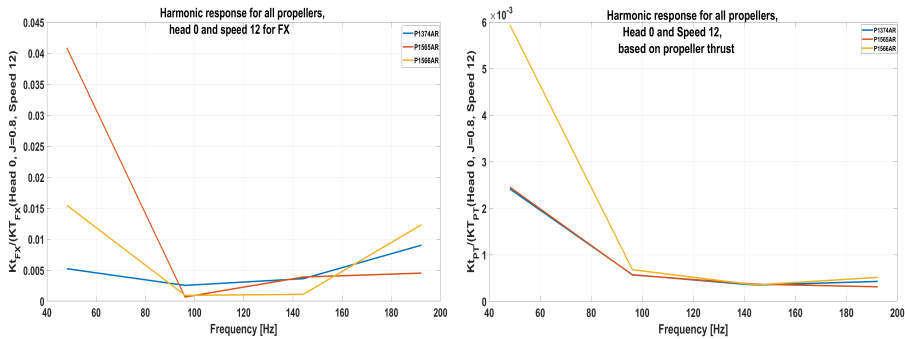


Figure 6.19: Harmonic Response for all Propellers at Zero Heading

Both figures include the effect of both skew angle and flexibility of the material, since the resin propellers are shown. Figure 6.20 shows the propeller thrust responses for the different rigid propellers.

### Comments on the Influence of Skew Angle

Figure 6.20 shows that the responses were dependent on the skew distribution, with differences at about 1% for higher advance ratios. However, compared to figures 6.18 and 6.19, it is clear that the skew angle mainly influenced the hydroelastic behaviour which affected the response.

For propeller thrust, except for the lowest advance ratio, the difference between

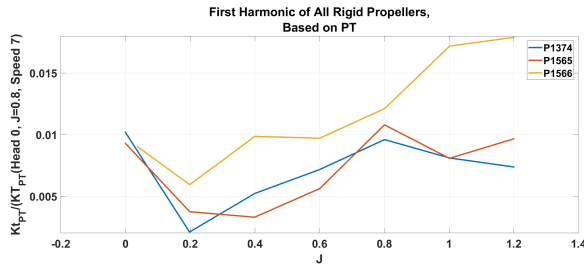


**Figure 6.20:** Harmonic Response for all Rigid Propellers

the different flexible propellers was small. At low advance ratios, the response for propeller P1566 with unbalanced skew was around 1.5% less than those of the other propellers. However, for higher advance ratios, this propeller had a higher response for both propeller rotational speeds.

The response for  $Fx\_vshaft$  was highest for propeller P1565AR, which does not have any skew, for both propeller rotational speeds. The largest difference was over 3%.

Propeller P1374 with balanced skew had the smallest changes in response with regards to both the advance ratio and the frequency. The peak in the response for FX in figure 6.17 was proposed to be due to noise in the previous section.

For the propeller with balanced skew, changing the hydrodynamic loading did not drastically affect the relative location of the pressure center and elastic axis. The changes in pitch distribution, and therefore in thrust, were small and steady. Similar reasoning is used to explain the behaviour of the propeller without skew, P1565. The location of its elastic axis and pressure center was significantly different compared to the propellers with skew, which could have led to higher responses.

### 6.3.6 Harmonics for Rigid Propellers Compared to Flexible Propellers

Figure 6.21 shows the harmonic responses for the rigid and flexible propeller. The response for FX is given with propeller P1565 for rotational speed 7 rps in straight ahead condition. The response based on propeller thrust is for P1566 at rotational speed 12 rps with azimuthing angle  $-10^\circ$ .

The difference in performance for the first harmonic was further evaluated. Figure 6.22 shows the difference in the first harmonic for all propellers at zero

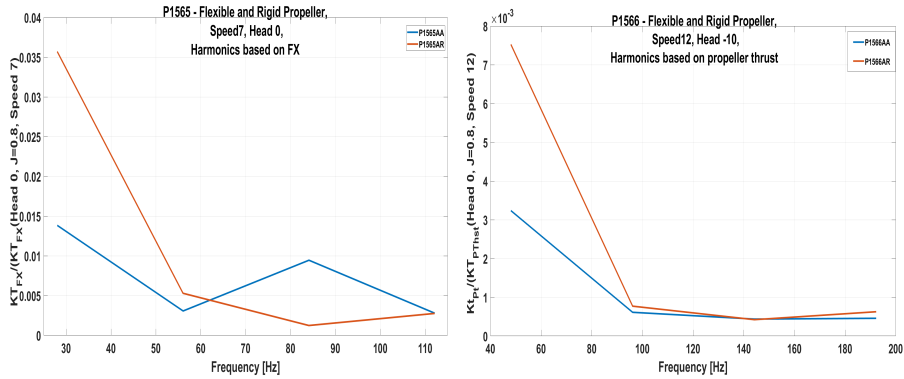


Figure 6.21: Harmonic Response for Rigid and Flexible Propellers

heading angle. This difference was found as  $\Delta K_T = K_T^{Rigid} - K_T^{Flexible}$ . A negative sign means therefore that the flexible propeller had a greater response than the rigid propeller.

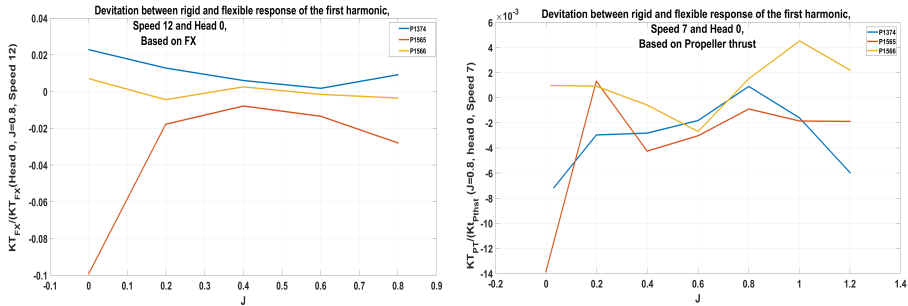


Figure 6.22: Deviation between Rigid and Flexible Propellers Harmonics at Zero Heading Angle

### Comments Regarding the Difference Between Rigid and Flexible Propeller Harmonics

The graphs in figure 6.21 show that there was a difference in response for rigid and flexible propellers. Largest difference occurred for the first harmonic, and in the displayed graphs, both responses were largest for the flexible propeller. When multiple propellers were evaluated, it was not possible to conclude that the flexible propeller had a larger response for the harmonics based on FX. That was however



possible for the harmonics based on propeller thrust. It was observed that the response for the flexible propeller was greater for the first harmonic. The difference was however small. Largest difference occurred for propeller P1565 at zero advance ratio where the first harmonic response of the flexible propeller was 1.4% higher than that of the rigid propeller.

Based on figure 6.22, it was seen that the difference between rigid and flexible propellers depended on the advance ratio and changed for different skew distributions. The difference was steady and small for a large range of advance ratios. At the lowest and highest advance ratios, the flexible propeller had in general a larger response. The skew distribution impacted the difference between the rigid and flexible propellers, as mentioned in section 6.3.5.

### 6.3.7 Harmonics at Azimuthing Headings

The harmonics of the propellers changed in different azimuthing conditions.

Figure 6.23 shows the first four harmonics of propeller P1566AR at the three azimuthing conditions. The propeller operated with advance ratio 0.8 at a rotational speed 7 rps.

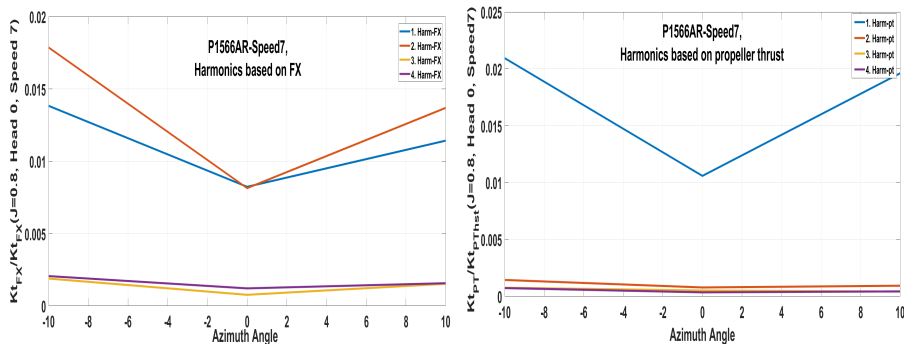


**Figure 6.23:** Harmonic Response for P1566AR at all Azimuth Headings

Figure 6.24 shows the first harmonic based on propeller thrust for all propellers in azimuthing condition with rotational speed 7 rps.

Figure 6.25 shows the difference in the first harmonics between rigid and flexible propellers for rotational speed 7 rps. All propellers are shown. The difference was found as  $\Delta K_T = K_T^{Rigid} - K_T^{Flexible}$ . A negative result means that the flexible propeller had a larger response than the rigid propeller.

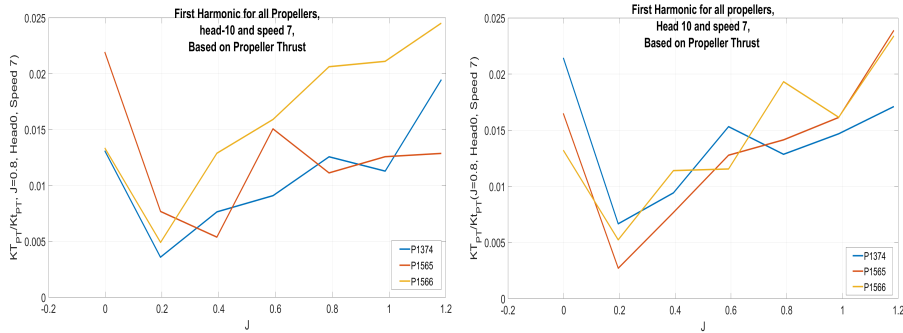


Figure 6.24: Harmonic Response based on Propeller Thrust for all Propellers

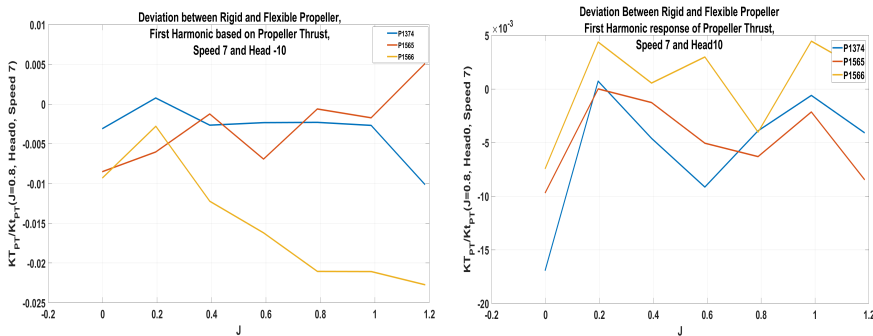


Figure 6.25: Deviation Between Rigid and Flexible Harmonic Response in Azimuth Conditions

### Comments Regarding the Azimuthing Heading

The interactions between the pod, strut and propeller are complex, and the complexity increases in azimuthing conditions.

The responses were lowest at zero heading angle. For the propeller thrust in figure 6.23, the first harmonic reponse at this heading was around half the size of the responses in the other directions. The propeller had an oblique inflow in azimuthing conditions, which affected the harmonic response.

Figure 6.24 is compared to figure 6.18 which shows the propeller thrust harmonics at zero heading. It is seen that the differences in response for the propellers were greater in azimuthing condition compared to straight ahead condition. A greater dependency on the advance ratio was observed, as the response of the propellers was up to 1% larger at the highest advance ratio compared to straight

ahead condition. At the advance ratio 0.2, that induced the smallest response, the changes were close to negligible.

The azimuthing conditions were seen influence the propellers differently. Figure 6.13 showed that propeller P1566 had the greatest response at  $-10^\circ$ , and similar as in straight ahead condition, this propeller had high responses for high advance ratios. This propeller had the largest difference between flexible and rigid propeller harmonic responses, shown in figure 6.25. The greatest difference was around 2.5%, and the flexible propeller had the largest response. This is different than for the time averaged propeller performance, for which the propeller had small relative differences in propeller thrust, shown in figure 6.9.

Propeller P1565 without skew had a low and steady harmonic response at  $-10^\circ$ , with a large response in bollard pull condition. At heading angle  $10^\circ$ , the response of this propeller was considerably larger and increased with the advance ratio. The difference in the responses between rigid and flexible propeller, shown in figure 6.25, was small. Large deviations occurred for high and low advance ratios. The difference in responses between the rigid and flexible propeller were similar in azimuthing conditions as for straight-ahead condition. These behaviours were different those of the averaged propeller performance shown in figure 6.9.

Propeller P1374 had a steadier response with the advance ratios. The difference between rigid and flexible propeller harmonics in figure 6.25 was small for this propeller. Larger differences for high and low advance ratios were also observed for this propeller.

The harmonic responses behaved significantly different than the average propeller performance, which indicates that important information vanishes when time-averaging the forces.

### **6.3.8 General Comments Regarding Larger Values in Response**

There are some responses which have a significant high magnitude. In general, largest responses occurred when the harmonic responses were calculated based on  $F_{x\_vshaft}$ . The highest response was 4.5% and occurred in figure 6.18 for propeller P1565. The RAOs for propeller P1374 were seen in the previous chapter, figure 5.7. The RAOs for propeller P1565AR and P1566AR are seen in figure 6.26.

Largest responses occurred for the first harmonics. Based on the RAOs of

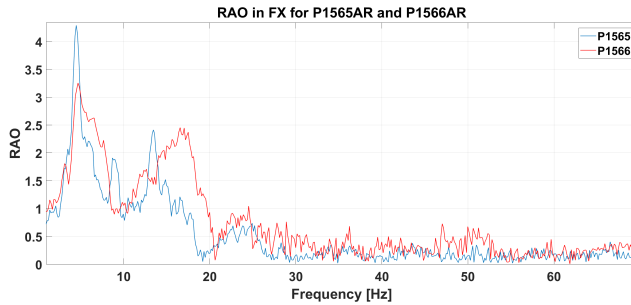


**Figure 6.26:** RAOs in FX for propeller P1565AR and P1566AR

the propeller, it is not possible to state that the eigenfrequencies led to the largest responses. Propeller P1565AR had the highest responses. It is shown in this thesis that this propeller had an altered propeller performance for higher hydrodynamic loads. It could be credible that this propeller had large responses, suggesting that it is difficult to operate flexible propellers with this skew distribution.

The propeller P1374 with balanced skew had in general the smallest response, with an exception for the FX response in figure 6.14. The response was around 4%. Figure 6.27 show all three repetitions for this condition.

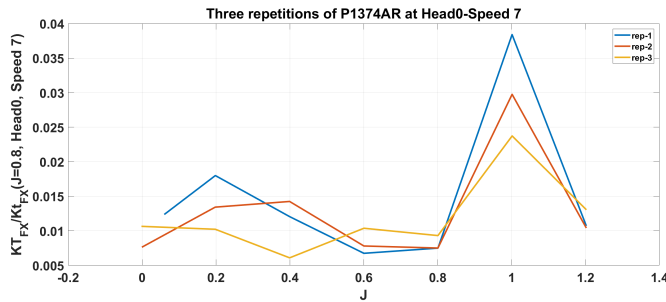


**Figure 6.27:** Three Repetitions for P1374AR

As the response decreased, it suggests that the first repetition was affected by noise. It is possible that noise have affected other responses.

## Conclusion

This thesis have presented the results from model tests of flexible propellers on a marine thruster. Three propellers with different skew distribution of rigid, aluminium material and of flexible, isotropic resin were tested. The propulsion unit was tested in three different azimuthing conditions with two different propeller rotational speeds. The changes in propeller performance and harmonic responses have been evaluated.

The flexible propellers were made of a resin material with a low elastic modulus, it therefore arose concerns that possible viscoelastic effects could occur. The repeatability of the propeller performance and harmonics have been evaluated. The changes in bollard pull conditions of the flexible propeller before and after a run was compared to that of the rigid propeller. The changes were small, in general less than 1%. The propellers regained its original shape after the run, and did not undergo any permanent or temporarily changes in geometry.

The propeller performance and harmonic responses were altered for the flexible propellers compared to the rigid propellers. The alteration was greater at high and low advance ratios. The azimuthing condition and the skew distribution affected the alteration. The flexible propellers had a reduced efficiency at high advance ratios. The propellers were not manufactured with an enhancement objective.

The skew distribution had an influence on the hydroelastic behaviour which affected the performance and harmonic response of the propellers. The propeller without any skew had considerable higher differences between rigid and flexible

propeller performance and harmonics at low advance ratios. The propeller with unbalanced skew had larger differences at high advance ratios. The propeller with balanced skew had smaller changes in propeller performance and harmonic responses. It is therefore reasonable to believe that propellers with balanced skew distribution is more beneficial to use with the marine thruster.

The azimuthing conditions affected the results. The headings affected the harmonic responses and propeller performance of the propellers differently. This indicates that by time-averaging the forces, important information regarding the propeller performance vanishes. It was seen that the heading angle  $-10^\circ$  had the largest influence on the propeller performance. No similar conclusion can be drawn for the harmonics. The propeller skew distribution affected the influence of the azimuthing conditions. .

## 7.1 Further Work

More research on flexible propellers on a marine thruster is necessary.

This model test experienced problems with the shaft, as it is unknown if it was strictly fixed for all runs. Uncertainties also arose with regards to the measurement channels in the vertical shaft. It was not possible to confirm that this affected the measurements. Nevertheless, it is recommended that one of the conditions is repeated to verify the results.

The thruster unit was designed with strict time limitations, and computational studies or optimization approaches were not done. The influence of thruster characteristics, as possible flow separation, on the propeller performance is therefore not known. It is recommended to evaluate this before using this thruster for further studies.

The results were seen to be significantly altered with the azimuthing conditions. A wider range of azimuthing conditions should be tested to analyze if the response increased linear with the heading angle. Due to the influence of the heading angle on the performance, all possible operational conditions should be controlled before operating a thruster with a flexible propeller.

The importance of the skew distribution on the performance has been shown. The propeller with balanced skew distribution had steadier variations in performance compared to the other propellers. A skew angle of  $23^\circ$  was tested. It is rea-

---

sonable to believe that this angle also influence the hydroelastic behaviour. Further studies are therefore recommended to alter the skew angle when having balanced skew distribution to further analyze the influence of skew.

The objective of the research project FlexProp, for which this thesis is a part of, is to demonstrate how hydroelastic effects can be taken into account to improve the design of thrusters and propellers, both by avoiding detrimental effects and achieving improved performance. The propellers that were used for this model test are made of an isotropic material and were designed without an optimization objective. It is recommended for further studies that the model tests are repeated with propellers with an anisotropic stacking sequence optimized for the bend-twist coupling. By doing this, it is therefore hoped the propulsion unit will have a performance enhancement.

# Bibliography

- Abramson, H. (1967), *Hydroelasticity with Special Reference to Hydrofoil craft*, Southwest Research Institute.
- Amini, H. (2011), Azimuth Propulsors in Off-design Conditions, PhD thesis, NTNU.
- Amini, H., Sileo, L. & Steen, S. (2012), ‘Numerical calculations of propeller shaft loads on azimuth propulsors in oblique inflow’, *Journal of Marine Science and Technology* .
- Amini, H. & Steen, S. (2011), ‘Loads on the azimuth propulsors shaft in oblique inflows and waves’, *International Journal of Maritime Engineering* .
- Amini, H., Steen, S. & Spence, J. (2010), ‘Shaft side force and bending moment on steerable thrusters in off-design conditions’, *International Symposium on Practical Design of Ships and Other Floating Structures, Rio, Brazil* .
- Carlton, J. (1994), *Marine Propellers and Propulsion*, Butterworth-Heinemann Publications.
- Das, H. & Kapuria, S. (2016), ‘On the use of bend-twist coupling in full-scale composite marine propellers for improving hydrodynamic performance’, *Journal of Fluids and Structures* 61 .
- Ghassemi, H. (2009), ‘The effect of wake flow and skew angle on the ship propeller performance’, *Mechanical Engineering Vol. 16* .



- 
- Ghassemi, H., Saryazdi, M. G. & Ghassabzadeh, M. (2012), 'Influence of the skew angle on the hydroelastic behaviour of a composite marine propeller', *Journal of Engineering for the Maritime Environment* .
- Harvald, S. (1983), *Resistance and Propulsion of Ships*, Wiley.
- Hoerner, S. F. (1965), *Fluid-Dynamic Drag, Practical Information on Aerodynamic Drag and Hydrodynamic Resistance*.
- Hong, Y., Wilson, P., He, X. & Wang, R. (2017), 'Numerical analysis and performance comparison of the same series of composite propellers', *Ocean Engineering* 144 pp. 211–223.
- Huang, Z., Xiong, Y. & Yang, G. (2016), 'Fluid-structure hydroelastic analysis and hydrodynamic cavitation experiments of composite propeller', *Proceedings of the Twenty-sixth International Ocean and Polar Engineering Conference Rhodes, Greece* .
- Islam, M. F. (2009), Performance Study of Podded Propulsors with Varied Geometry and Azimuthing Conditions, PhD thesis, Memorial University of Newfoundland.
- Islam, M., Veitch, B., Akinturk, A., Bose, N. & Liu, P. (2009), 'Performance study of podded propulsor in static and azimuthing conditions', *International Shipbuilding Progress* 56 .
- Islam, M., Veitch, B. & Liu, P. (2008), 'Experimental research on marine podded propulsors', *Journal of Naval Architecture and Marine Engineering* .
- Khan, M., Adams, D. O., Dayal, V., & Vogel, J. M. (2000), 'Effects of bend-twist coupling on composite propeller performance', *Mechanics of Composite Materials and Structures* 7 .
- Lee, H., Song, M.-C., Suh, J., Cha, M. & Chanf, B. (2015), 'A numerical study on the hydro-elastic behavior of composite marine propeller', *Fourth International Symposium on Marine Propulsors, smp'15, Austin, Texas, USA* .
- Lin, C.-C., Lee, Y.-J. & Hung, C.-S. (2009), 'Optimization and experiment of composite marine propellers', *Composite Structures* 89 .

- 
- Lin, H. & Tsai, J. (2008), 'Analysis of underwater free vibrations of a composite propeller blade', *Journal of Reinforced Plastics and Composites* 27 .
- Liu, Z. & Young, Y. L. (2007), 'Utilization of deformation coupling in self-twisting composite propellers', *Proceedings of 16th International Conference on Composite Materials, Kyoto, Japan* .
- Maljaars, P., Bronswijk, L., Windt, J., Grasso, N. & Kaminski, M. (2018), 'Experimental validation of fluidstructure interaction computations of flexible composite propellers in open water conditions using bem-fem and rans-fem methods', *Journal of Marine Science and Engineering* .
- Maljaars, P. & Dekker, J. (2015), 'Hydro-elastic analysis of flexible marine propellers', *Maritime Technology and Engineering* .
- Maljaars, P. J. & Kaminski, M. L. (2015), 'Hydro-elastic analysis of flexible propellers: an overview', *4th International Symposium on Marine Propulsors* .
- Molloy, S., He, M., Islam, M., Veitch, B., Bose, N. & Liu, P. (2006), 'Hydrodynamic study of podded propulsors with systematically varied geometry', *T-Pod* .
- Motley, M., Liu, Z. & Young, Y. (2009), 'Utilizing fluid-structure interactions to improve energy efficiency of composite marine propellers in spatially varying wake', *Composite Structures* 90 .
- Nieminen, V. (2017), 'Hydro-elastic analysis of a propeller using cfd and fem co-simulation', *Fifth International Symposium on Marine Propulsors, smp'17, Espoo, Finland* .
- Paik, B., Kim, G., Kim, K. Seol, H., Hyun, B., Lee, S. & Jung, Y. (2013), 'Investigation on the performance characteristics of the flexible propellers', *Ocean Engineering* .
- Papanicolaou, G. & Zaoutsos, S. (2011), 'Viscoelastic constitutive modeling of creep and stress relaxation in polymers and polymer matrix composites', *Creep and Fatigue in Polymer Matrix Composites* .

- 
- Savio, L. (2015), 'Measurements of the deflection of a flexible propeller blade by means of stereo imaging', *Fourth International Symposium on Marine Propulsors smp15, Austin, Texas, USA* .
- Savio, L. & Koushan, K. (2019), 'Open water characteristics of three model scale flexible propellers', *VIII International Conference on Computational Methods in Marine Engineering, MARINE* .
- Savio, L., Sileo, L., Steen, S., Glodowski, R., Hoffmann, P. & Kraskowski, M. (2011), 'Comparison of experimental and numerical predictions of open water performance characteristics of a podded propeller', *Advanced Model Measurement Technology for EU Maritime Industry* .
- Steen, S. (2014a), *Lecture notes, TMR4200 Naval Hydrodynamics*.
- Steen, S. (2014b), *Lecture notes, TMR7-Experimental Methods in Marine Hydrodynamics*.
- Taketani, T., Kimura, K., Ando, S. & Yamamoto, K. (2013), 'Study on performance of a ship propeller using a composite material', *Third International Symposium on Marine Propulsors smp13, Launceston, Tasmania, Australia* .
- Young, Y. (2008), 'Fluid-structure interaction analysis of flexible composite marine propellers', *Journal of Fluids and Structures* .
- Young, Y. L., Garg, N., Brandner, P. A., Pearce, B. W., Butler, D., Clarke, D. & Philips, A. W. (2018), 'Load-dependent bend-twist coupling effects on the steady-state hydroelastic response of composite hydrofoils', *Composite Structures* 189 .
- Zhang, Q. & Hisada, T. (2004), 'Studies of the strong coupling and weak coupling methods in fsi analysis', *International Journal for Numerical Methods in Engineering* 60 .



---

# Appendix

## 7.2 Propeller Geometry

### 7.2.1 P1374

**Table 7.1:** Main Geometrical Parameter of Propeller P1374

<b>r/R</b>	<b>r</b>	<b>Lfor</b>	<b>Laft</b>	<b>b</b>	<b>cs</b>	<b>xr</b>	<b>eo</b>	<b>fo</b>	<b>P</b>	<b>Fi</b>
-	mm	mm	mm	mm	mm	mm	mm	mm	mm	deg
0.24	30	16.67	-16.67	33.35	0	0	9.51	0.27	268.5	55.03
0.25	31.25	18.12	-17.22	35.34	0.45	0	9.38	0.85	269.74	53.95
0.3	37.5	25.21	-19.78	44.99	2.71	0	8.68	1.69	270.84	48.98
0.35	43.75	31.96	-22.13	54.09	4.91	0	8	2.19	271.81	44.68
0.4	50	38.26	-24.34	62.6	6.96	0	7.35	2.56	272.66	40.96
0.5	62.5	48.98	-28.62	77.6	10.18	0	6.12	3.08	273.96	34.9
0.6	75	55.93	-33.46	89.39	11.24	0	5	3.35	274.74	30.24
0.7	87.5	57.33	-39.65	96.98	8.84	0	3.98	3.36	275	26.57
0.8	100	50.68	-47.81	98.49	1.44	0	3.05	3	272.05	23.41
0.9	112.5	31.88	-57.23	89.1	-12.68	0	2.23	2.08	259.41	20.15
0.95	118.75	14.71	-60.34	75.05	-22.81	0	1.85	1.35	248.38	18.41
0.975	121.88	1.87	-59.42	61.29	-28.77	0	1.68	0.9	241.52	17.51
0.99	123.75	-9.69	-55.61	45.92	-32.65	0	1.56	0.54	236.97	16.95
0.995	124.38	-15.66	-52.31	36.65	-33.99	0	1.54	0.38	235.39	16.76
1	125	-25.99	-44.74	18.75	-35.36	0	1.5	0	233.75	16.57

---

## 7.2.2 P1565

**Table 7.2:** Main Geometrical Parameter of Propeller P1565

<b>r/R</b>	<b>r</b>	<b>Lfor</b>	<b>Laft</b>	<b>b</b>	<b>cs</b>	<b>xr</b>	<b>eo</b>	<b>fo</b>	<b>P</b>	<b>Fi</b>
-	mm	mm	mm	mm	mm	mm	mm	mm	mm	deg
0.24	30	16.67	-16.67	33.35	0	0	9.51	0.28	269.5	55.03
0.25	31.25	17.67	-17.67	35.34	0	0	9.38	0.85	269.74	53.95
0.3	37.5	22.49	-22.49	44.99	0	0	8.68	1.69	270.84	48.98
0.35	43.75	27.04	-27.04	54.09	0	0	8	2.19	271.81	44.68
0.4	50	31.3	-31.3	62.6	0	0	7.35	2.56	272.66	40.96
0.5	62.5	38.8	-38.8	77.6	0	0	6.12	3.08	273.96	34.9
0.6	75	44.69	-44.69	89.39	0	0	5	3.35	274.74	30.24
0.7	87.5	48.49	-48.49	96.98	0	0	3.98	3.36	275	26.57
0.8	100	49.24	-49.24	98.49	0	0	3.05	3	272.05	23.41
0.9	112.5	44.55	-44.55	89.1	0	0	2.23	2.08	259.41	20.15
0.95	118.75	37.53	-37.53	75.05	0	0	1.85	1.35	248.38	18.41
0.975	121.88	30.64	-30.64	61.29	0	0	1.68	0.9	241.52	17.51
0.99	123.75	22.96	-22.96	45.92	0	0	1.56	0.54	236.97	16.95
0.995	124.38	18.32	-18.32	36.65	0	0	1.54	0.38	235.39	16.76
1	125	9.38	-9.38	18.75	0	0	1.5	0	233.75	16.57

### 7.2.3 P1566

**Table 7.3:** Main Geometrical Parameter of Propeller P1566

<b>r/R</b>	<b>r</b>	<b>Lfor</b>	<b>Laft</b>	<b>b</b>	<b>cs</b>	<b>xr</b>	<b>eo</b>	<b>fo</b>	<b>P</b>	<b>Fi</b>
-	mm	mm	mm	mm	mm	mm	mm	mm	mm	deg
0.24	30	16.67	-16.67	33.35	0	0	9.51	0.28	269.5	55.03
0.25	31.25	17.39	-17.95	35.34	-0.28	0	9.38	0.85	269.74	53.95
0.3	37.5	20.68	-24.3	44.99	-1.81	0	8.68	1.69	270.84	48.98
0.35	43.75	23.47	-30.62	54.09	-3.58	0	8	2.19	271.81	44.68
0.4	50	25.71	-36.9	62.6	-5.59	0	7.35	2.56	272.66	40.96
0.5	62.5	28.34	-49.27	77.6	-10.46	0	6.12	3.08	273.96	34.9
0.6	75	28.19	-61.2	89.39	-16.51	0	5	3.35	274.74	30.24
0.7	87.5	24.72	-72.26	96.98	-23.77	0	3.98	3.36	275	26.57
0.8	100	17.01	-81.48	98.49	-32.23	0	3.05	3	272.05	23.41
0.9	112.5	2.77	-86.33	89.1	-41.78	0	2.23	2.08	259.41	20.15
0.95	118.75	-9.41	-84.46	75.05	-46.94	0	1.85	1.35	248.38	18.41
0.975	121.88	-18.97	-80.26	61.29	-49.61	0	1.68	0.9	241.52	17.51
0.99	123.75	-28.29	-74.21	45.92	-51.25	0	1.56	0.54	236.97	16.95
0.995	124.38	-33.47	-70.12	36.65	-51.8	0	1.54	0.38	235.39	16.76
1	125	-42.98	-61.73	18.75	-52.35	0	1.5	0	233.75	16.57

## 7.2.4 Blade Section Profiles for P1374, P1565, P1566

Blade section profiles

x/b-chordwise coordinate

Yu, Yl - ordinates of the upper/lower sides of the profile

Yc - ordinates of the profile mean line

	x/b	0	0.005	0.0075	0.0125	0.025	0.05	0.1	0.2	0.3	0.4	0.5	0.6	0.7	0.8	0.9	0.95	1
0.24	Yu	0	0.65	0.81	1.05	1.47	2.06	2.86	3.89	4.53	4.91	5.03	4.9	4.42	3.52	2.1	1.24	0.3
	Yl	0	-0.62	-0.77	-1	-1.39	-1.91	-2.62	-3.5	-4.06	-4.38	-4.48	-4.36	-3.93	-3.14	-1.9	-1.14	-0.3
	Yc	0	0.01	0.02	0.03	0.04	0.07	0.12	0.19	0.24	0.26	0.28	0.27	0.25	0.19	0.1	0.05	0
0.25	Yu	0	0.66	0.83	1.09	1.55	2.19	3.08	4.24	4.97	5.39	5.54	5.39	4.87	3.88	2.29	1.34	0.3
	Yl	0	-0.59	-0.73	-0.93	-1.28	-1.73	-2.32	-3.05	-3.5	-3.75	-3.83	-3.72	-3.36	-2.68	-1.66	-1.02	-0.3
	Yc	0	0.04	0.05	0.08	0.14	0.23	0.38	0.6	0.74	0.82	0.85	0.83	0.76	0.6	0.31	0.16	0
0.3	Yu	0	0.65	0.82	1.09	1.57	2.27	3.26	4.56	5.38	5.86	6.03	5.88	5.32	4.23	2.46	1.42	0.3
	Yl	0	-0.51	-0.62	-0.78	-1.04	-1.35	-1.74	-2.19	-2.45	-2.6	-2.64	-2.56	-2.3	-1.85	-1.21	-0.8	-0.3
	Yc	0	0.07	0.1	0.15	0.27	0.46	0.76	1.18	1.46	1.63	1.69	1.66	1.51	1.19	0.62	0.31	0
0.35	Yu	0	0.63	0.79	1.06	1.55	2.27	3.28	4.64	5.5	6.01	6.19	6.03	5.46	4.35	2.51	1.44	0.3
	Yl	0	-0.44	-0.53	-0.66	-0.86	-1.08	-1.32	-1.58	-1.72	-1.8	-1.81	-1.75	-1.57	-1.27	-0.9	-0.64	-0.3
	Yc	0	0.09	0.13	0.2	0.35	0.59	0.98	1.53	1.89	2.1	2.19	2.14	1.94	1.54	0.81	0.4	0
0.4	Yu	0	0.6	0.76	1.02	1.51	2.23	3.26	4.65	5.53	6.05	6.23	6.08	5.5	4.38	2.52	1.44	0.3
	Yl	0	-0.38	-0.46	-0.56	-0.7	-0.84	-0.97	-1.07	-1.11	-1.13	-1.12	-1.07	-0.95	-0.79	-0.64	-0.5	-0.3
	Yc	0	0.11	0.15	0.23	0.41	0.69	1.15	1.79	2.21	2.46	2.56	2.5	2.27	1.8	0.94	0.47	0
0.5	Yu	0	0.54	0.69	0.94	1.41	2.11	3.14	4.53	5.42	5.95	6.14	5.99	5.42	4.32	2.48	1.41	0.3
	Yl	0	-0.28	-0.33	-0.38	-0.43	-0.45	-0.39	-0.23	-0.11	-0.03	0.01	0.03	0.05	0	-0.21	-0.28	-0.3
	Yc	0	0.13	0.18	0.28	0.49	0.83	1.38	2.15	2.66	2.96	3.08	3.01	2.74	2.16	1.13	0.57	0
0.6	Yu	0	0.47	0.61	0.84	1.28	1.95	2.94	4.28	5.15	5.66	5.85	5.71	5.17	4.13	2.36	1.35	0.3
	Yl	0	-0.19	-0.22	-0.24	-0.22	-0.14	0.06	0.4	0.63	0.78	0.85	0.85	0.78	0.58	0.11	-0.11	-0.3
	Yc	0	0.14	0.2	0.3	0.53	0.91	1.5	2.34	2.89	3.22	3.35	3.28	2.98	2.35	1.23	0.62	0
0.7	Yu	0	0.41	0.53	0.73	1.13	1.74	2.65	3.89	4.69	5.17	5.34	5.22	4.73	3.78	2.16	1.25	0.3
	Yl	0	-0.12	-0.13	-0.12	-0.07	0.08	0.36	0.8	1.1	1.29	1.37	1.35	1.24	0.94	0.31	-0.01	-0.3
	Yc	0	0.14	0.2	0.3	0.53	0.91	1.5	2.35	2.9	3.23	3.36	3.28	2.98	2.36	1.24	0.62	0
0.8	Yu	0	0.33	0.43	0.6	0.93	1.45	2.22	3.28	3.96	4.37	4.52	4.42	4	3.21	1.85	1.09	0.3
	Yl	0	-0.08	-0.08	-0.06	0.02	0.17	0.46	0.91	1.21	1.39	1.47	1.45	1.33	1	0.36	0.02	-0.3
	Yc	0	0.13	0.18	0.27	0.48	0.81	1.34	2.1	2.59	2.88	3	2.93	2.66	2.11	1.1	0.55	0
0.9	Yu	0	0.24	0.31	0.43	0.66	1.03	1.57	2.32	2.8	3.08	3.19	3.11	2.82	2.28	1.35	0.83	0.3
	Yl	0	-0.06	-0.06	-0.05	-0.01	0.1	0.29	0.59	0.79	0.91	0.96	0.95	0.87	0.64	0.18	-0.07	-0.3
	Yc	0	0.09	0.12	0.19	0.33	0.56	0.93	1.45	1.79	2	2.08	2.03	1.85	1.46	0.77	0.38	0
0.95	Yu	0	0.18	0.23	0.32	0.49	0.75	1.14	1.66	2	2.2	2.28	2.22	2.01	1.64	1.02	0.66	0.3
	Yl	0	-0.07	-0.07	-0.08	-0.06	-0.02	0.07	0.23	0.33	0.4	0.43	0.42	0.39	0.26	-0.02	-0.16	-0.3
	Yc	0	0.06	0.08	0.12	0.21	0.37	0.61	0.95	1.17	1.3	1.35	1.32	1.2	0.95	0.5	0.25	0
0.975	Yu	0	0.15	0.19	0.26	0.39	0.59	0.89	1.28	1.53	1.68	1.74	1.69	1.53	1.26	0.82	0.56	0.3
	Yl	0	-0.07	-0.09	-0.1	-0.11	-0.11	-0.08	-0.02	0.02	0.05	0.06	0.06	0.06	0	-0.15	-0.23	-0.3
	Yc	0	0.04	0.05	0.08	0.14	0.24	0.4	0.63	0.78	0.86	0.9	0.88	0.8	0.63	0.33	0.17	0
0.99	Yu	0	0.13	0.16	0.22	0.32	0.47	0.69	0.98	1.17	1.28	1.32	1.29	1.17	0.97	0.66	0.48	0.3
	Yl	0	-0.08	-0.1	-0.12	-0.15	-0.18	-0.21	-0.23	-0.24	-0.24	-0.24	-0.23	-0.21	-0.21	-0.26	-0.28	-0.3
	Yc	0	0.02	0.03	0.05	0.09	0.15	0.24	0.38	0.47	0.52	0.54	0.53	0.48	0.38	0.2	0.1	0
0.995	Yu	0	0.12	0.15	0.2	0.29	0.42	0.61	0.86	1.02	1.11	1.15	1.12	1.01	0.85	0.6	0.45	0.3
	Yl	0	-0.09	-0.11	-0.13	-0.17	-0.22	-0.27	-0.33	-0.37	-0.39	-0.39	-0.38	-0.34	-0.32	-0.32	-0.31	-0.3
	Yc	0	0.02	0.02	0.03	0.06	0.1	0.17	0.26	0.33	0.36	0.38	0.37	0.33	0.26	0.14	0.07	0
1	Yu	0	0.1	0.12	0.16	0.23	0.31	0.43	0.58	0.68	0.73	0.75	0.73	0.66	0.56	0.42	0.34	0.25
	Yl	0	-0.1	-0.12	-0.16	-0.23	-0.31	-0.43	-0.58	-0.68	-0.73	-0.75	-0.73	-0.66	-0.56	-0.42	-0.34	-0.25
	Yc	0	0	0	0	0	0	0	0	0	0	0	0	0	0	0	0	0



---

## 7.3 Channel List

Channel	Name	Unit	Sample Frequency	Zero Value	Filter
1	DAQ time stamps	s	200	0	–
2	DAQ time stamps SR2	s	9600	0	–
3	DAQ time stamps absolute	hh:mm:ss	200	0	–
4	DAQ time stamps absolute SR2	hh:mm:ss	9600	0	–
5	Speed	m/s	200	0	Bu 20 Hz
6	NTP time stamps QX	s	Inf	0	Bu 20 Hz
7	Speed_analog_PLS	m/s	200	0	Bu 20 Hz
8	Vogn_pos	m	200	0	Bu 20 Hz
9	ACC_X_T HR	$m/s^2$	9600	78.52	Bu 20 Hz
10	Fy_Total	N	9600	-133.32	Bu 1000 Hz
11	acqstatus	V	200	0	Bu 50 Hz
12	NTP time stamps QX SR2	s	9600	0	Bu 20 Hz
13	P_thrust	N	9600	-179.05	Bu 1000 Hz
14	P_torque	Nm	9600	6.49	Bu 1000 Hz
15	20561_fx	mV	9600	0.2098	Bu 1000 Hz
16	20561_fy	mV	9600	0.2840	Bu 1000 Hz
17	20561_mx	mC	9600	-1.09	Bu 1000 Hz
18	T_thrust	N	9600	-51.20	Bu 1000 Hz
19	Hammer_Force	N	9600	-173.36	Bu 1000 Hz
20	P_rev	Hz	200	0	Bu 20 Hz
21	Fx_vshaft	N	9600	0	–
22	Fy_vshaft	N	9600	0	–
23	Mz_vshaft	Nm	9600	0	–
24	Angle_Thrust	deg	9600	0	–

---

## 7.4 Run Matrix

1xxxx	P1374AA
2xxxx	P1374AR
3xxxx	P1565AA
4xxxx	P1565AR
5xxxx	P1566AA
6xxxx	P1566AR
x0xxx	Propeller rotational speed 7 rps
x2xxx	Propeller rotational speed 12 rps
xx0xx	Azimuthing angle $0^\circ$
xx1xx	Azimuthing angle $-10^\circ$
xx2xx	Azimuthing angle $10^\circ$
xxxx0	First repetition
xxxx1	Second repetition
xxxx2	Third repetition

---

## 7.5 Symbols used for the Results

AA	Represents aluminium propellers
AR	Represents resin propellers
Head 0	Straight ahead condition
Head -10	Azimuthing angle $-10^\circ$
Head 10	Azimuthing angle $10^\circ$
P_thrust	Propeller thrust
P_torque	Propeller torque
Fx_vshaft	Propulsion unit thrust from vertical shaft
Fy_vshaft	Propulsion unit thrust in y-direction from vertical shaft
T_thrust	Propulsion unit thrust measured above unit
$Kt_{Prop}$	Thrust coefficient based on P_thrust
$Kt_{vshaft}$	Thrust coefficient based on Fx_vshaft
$Kt_{Thruster}$	Thrust coefficient based on T_thrust
$\eta_{prop}$	Efficiency based on propeller thrust
$\eta_{unit}$	Efficiency based on propulsion unit thrust
$K_Q$	Torque coefficient
delta $Kt_{prop}$	Difference in rigid and flexible thrust coefficient based on P_thrust
delta $Kt_{thruster}$	Difference in rigid and flexible thrust coefficient based on T_thrust
FX	Harmonics are based on Fx_vshaft
FY	Harmonics are based on Fy_vshaft
PT	Harmonics are based on P_thrust

